# The Quartz Lamella Fabrics in a Concentric Fold

By

**Ikuo HARA**

*with 1 Table, 26 Text-figures, and 7 Plates*

ABSTRACT: Lamellar structures in quartz grains occurring in a concentric fold (multiple-layered system made of the alternation of mica-rich layers and quartz-rich layers) found in the Sangun metamorphic formation at Atetsu, Okayama Pref., Southwest Japan, have been described. Two types of lamellar structure have been found in quartz grains of the quartz-rich layers, that is, the Böhm lamellae and the deformation bands. The crystallographic location of the deformation bands has been tentatively determined on the basis of assumption that the rotational axis of the change in the lattice orientation from the band to the host crystal coincides with either the a-axis or the a*-axis. At this time the deformation bands show a wide range of the crystallographic location, but many of them are inclined at high angles to the c-axis. Quartz grains containing the deformation bands are found in very sharply restricted parts in the fold, and these parts all correspond approximately to the "knee of fold". The distribution of quartz grains containing the Böhm lamellae is also sharply restricted in two narrow zones through the fold, which are approximately placed on the knee of fold, though the distribution area is more enlarged to the limbs than that for the deformation bands. The Böhm lamellae occurring in the central part of the knee are different in geometric properties from those occurring in the marginal parts of the knee and in the limbs. Namely, most of the former is inclined at high angles to the c-axis, and, in the diagram for the pole of lamellae and the c-axis for the former, great circles containing these axial data for individual grains have a constant direction and sense, while the latter shows a wide range of the crystallographic location and the diagram in question does not show any regularity. In the specimens described so far in the literature, the Böhm lamellae referred to the type of the former and these to the type of the latter appear to be commonly coexisting. The rule for establishing the directions of the principal normal stresses developed in the system concerned during the deformation related to the formation of the lamellae, previously introduced by the author (1961a and 1963), has been successfully used also for the present specimen. The cause of the fact that quartz grains containing the deformation bands or the Böhm lamellae are found in some very sharply restricted parts in the fold (especially the "knee of fold") has been also discussed with reference to the mechanics of rock folding in the final phase of metamorphic deformation.

CONTENTS

## I. INTRODUCTION

Recently the nature of the lamellar structures in quartz and theories of their origin have been comprephensively reviewed by CHRISTIE *et al.* (1959) and TURNER *et al.* (1963). These authors have realized that our present knowledge on the structure in question is not always adequate for any rigorous treatment of its dynamic significance. In this paper, the present author will describe in greater detail the quartz lamella fabrics in a small-scale fold found in the Sangun metamorphic formation at Atetsu, Okayama Pref., Southwest Japan, paying regard to their dynamic significance. Described data will also have some contributions to the knowledge of the mechanics of rock folding in the final phase of metamorphic deformation.

ACKNOWLEDGEMENTS: The author wishes to record his sincere thanks to Prof. G. KOJIMA, who read this manuscript and offered valuable criticisms. Thanks are due to the members of the Petrologist Club of the Hiroshima University for their valuable discussions. Finally the author acknowledges with gratitude that a part of the expense for this research was defrayed by the Grant in Aid for Scientific Reseaches from the Ministry of Education, Japan.

## II. STYLE OF FOLD

The rock involved in the fold examined in this paper is a crystalline schist derived from siliceous shale, and it consists mainly of quartz and muscovite, accompanied with subordinate carbonaceous matter, chlorite and albite. The rock in question is characterized by a single distinct foliation defined by alternation of muscovite-rich layers and quartz-rich layers, that defines the form of the fold, (multiple-layered system), and by a lineation (parallel grooves on the faliation) parallel to the axis of the fold. Boundaries between the mica-rich layers and quartz-rich layers are commonly sharply drawn by a line on the plane of the thin section normal to the fold-axis (*e. g.* Plate 35-1), and thickness of the former and of the latter do not exceed 5 mm.

The profile of the fold in question and its environs observed in the field shows distinct two zones, that is, in one of the zones the layers are folded in an acute or open form (folded zone) and in the other zone the layers are not so folded (non-folded zone). The boundary between the folded zone and the non-folded zone is clearly drawn along the surface of décollement which means the detachment of the former from the latter. Broadly speaking, folds in the folded zone are defined in terms of folds of an acute or open form with wave-length between 2 cm and 10 cm, whose axial planes are subparallel to each other and standing at high angles on the boundary surface between the folded and the non-folded zone, and which share the same fold-axis in common. They have macroscopically a monoclinic symmetry with a single symmetry plane normal to the fold-axis. The fold system (the folded zone)

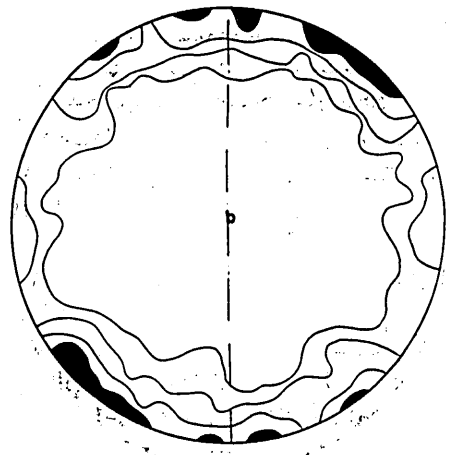

Fig. 1 [001] -axes of 300 mica flakes in the quartz-rich layers. broken line: the axial plane of the fold. Contour: 5-3-2-1%

which consists of those folds has a monoclinic symmetry. The fold examined in this paper is one of them.

Muscovite flakes occurring sporadically in the quartz-rich layers are generally oriented parallel to the foliation surface (the form surface of the fold) (*e.g.* Plate 35–1). The [001] -axis fabric for mucovite flakes in the quartz-rich layers was examined throughout the fold and was collectively shown in Fig. 1. The mica fabric is characterized by a sharply defined great circle girdle, showing a monoclinic symmetry with a single symmetry axis normal to the girdle. The symmetry axis represents the fabric axis b for the mica fabric and is correlated with the axis of the fold in question.

Plate 34–1 is a sketch of the fold in question on the ac thin section. It represents that the same fold-style is not uniformly developed through individual layers involved in the fold, but that with reference to fold-style of individual layers the fold may be divided into the following three units: 1) fold A consisting of layers b, c, d, e, f, g, h and i, 2) fold B consisting of layers j, k, l, m, n, o, p, q, and r, and 3) fold C consisting of layers s, t, u, v, w, x, y and z and of overlying others on Plate 34–1.

Some characteristics of fold A are enumarated as follows: 1) In the innermost knee, layer b shows reverse folding with respect to other overlying layers and in the boundary between layer b and layer c occurs an unique part consisting of coarse granular grains of quartz, whose c-axes demonstrate random orientation (Fig. 3), unlike tabular grains of quartz in the surrounding quartz-rich layers b and d which represent preferred lattice and dimensional orientation described in later pages (Plate 37–4). 2) Layers c to i are sharply buckled at acute angles along the short knee. 3) In both limbs layers d to h are gently bent in concave form on Plate 34–1. And 4) the thickness of layers b to i, measured radially, is not always constant, but the layers tend to become thicker toward the axial part of the fold. Especially in the fold of

mica-rich layers c this tendency is pronounced, as shown in Plates 34-1 and 37-4.

Some characteristics of fold B are enumerated as folldws; 1) open form, and 2) constant thickness, measured radially, except the mica-rich layer q which is slightly thickened toward the axial part. Style of fold B inferred from the above-described characteristics is different from that of fold A, representing marked discrepancy between the former and the latter in relation to the stress system developed during folding.

Some characteristics of fold C are enumerated as follows: 1) The layers are all sharply buckled at acute angles along the short knee. 2) At the knee is found a surface of décollement along the axial plane, which acted as a surface of detachment between the left side and the right side of the axial plane. 3) In both limbs the layers are gently bent in concave form on Plate 34-1. For convenience' sake, the reversed folds in the limbs of fold C are designated as fold C′ (right limb) and fold C″ (left limb) respectively. And 4) the thickness of layers, measured radially, is not constant, but generally becomes thicker toward the axial part. Style of fold C inferred from the above-described characteristics is essentially the same as that of fold A mentioned above. The fold-style of the former as well as the latter seems to indicate that the layers involved in them were strongly compressed normal to their axial plane and to the fold-axis (*cf.* de SITTER, 1956).

In the mica-rich layers mica flakes tend to be preferably oriented parallel to the foliation surface, defining a distinct schistosity. But, in most of them are found slip cleavages traversing the schistosity surface at various angles. The transversal slip cleavages develop through the fold in such a fashion as shown in Plate 34-1. It can be pointed out that they are mainly developed in the mica-rich layers involved in fold A and fold C. Broadly speaking, in the axial part they traverse the schistosity surface at high angles and they are arranged in a fan-like manner about the axial plane, and on the limbs they tend to run subparallel to the foliation surface. Generally, the transversal slip cleavages do not cut across the quartz-rich layers.

Dimensional fabric of quartz grains in the quartz-rich layers, examined on the thin section normal to the fold-axis, is not homogeneous. Broadly speaking, many of quartz grains seem to be preferably oriented with their longest dimension parallel to the foliation surface and show tabular habit, except quartz grains in layer b and in Fq zones which will be mentioned in the following paragraphs, (Fig. 2 and Table 1). In layer b many of quartz grains are preferably oriented with their longest dimension parallel or subparallel to the axial plane of fold A (Fig. 2).

In layers h, j, p, r, t, v, w, x, y and z and overlying others are found narrow zones consisting of coarse granular grains of quartz which are generally different in shape and dimension from quartz grains with tabular habit in the host quartz-rich layers (Plates 35-2, 3 and 4, 36-4, and 37-3). Width of those zones is less than 1 mm. They traverse straightly the foliation surface at high angles, in many cases terminating within the quartz-rich layers. The mica-rich layers which are cut by those zones are commonly very thin. As shown in Plates 35-1, 3 and 4, 36-3 and 37-3, generally,

in those zones are scarcely present mica flakes oriented parallel to the foliation of the host layer. The zones having some characteristics enumerated above are designated as Fq zone. The distribution of the Fq zones through the fold is shown in Plate 34-1. It can be pointed out that the Fq zones (1 to 8 in Plate 34-1) are distributed in restricted parts of the fold, that is, in some parts of the limbs of fold B and also of fold C which correspond to the knee of fold C′ and fold C″.

In the left limbs of fold C occurs a narrow zone consisting of fine granular grains of quartz which traverses straightly at high angles the host layers (Fq zone 10 in Plate 34-1). Quartz grains in this zone are finer-grained than those in the host quartz-rich layers. As shown in Plate 36-1 and 2, in this zone are scarcely present mica flakes oriented parallel to the foliation surface of the host layer, but along the boundary between the zone and host layer is found row of minute dark materials and minute flaky mineral grains.

In the right limb of fold of the layers l, m, n, o, p and r occurs an unique zone (Fq zone 9 in Plate 34-1) which traverses those layers at high angles. This zone shows a zonal structure comprising two subzones: The one consists of coarse granular grains of quartz whose texture is identical with that of the Fq zones, and the other is displayed as row of voids free from even quartz and other mineral grains, though walls of the voids are coated with minute dark materials and minute flaky mineral grains (Plate 37-1 and 2).

In the left limb of fold of the quartz-rich layer j are recognized planar structures

Table 1. Summary of the dimensional orientation data[1]

| Locality (No. Sectors) | Vector Azimuth (Angle from S)[2] | Vector Magnitude | Probability | Significant[3] |
|---|---|---|---|---|
| | (Degrees) | (Per cent) | | |
| 1 | 3° | 79 | $<10^{-10}$ | Yes |
| 2* | 1° | 69 | $<10^{-10}$ | Yes |
| 3* | 0° | 68 | $<10^{-10}$ | Yes |
| 4 | 0° | 91 | $<10^{-15}$ | Yes |
| 5 | 4° | 89 | $<10^{-15}$ | Yes |
| 6 | 2° | 77 | $<10^{-10}$ | Yes |
| 7 | 0° | 97 | $<10^{-20}$ | Yes |
| 8* | −3° | 65 | $<10^{-5}$ | Yes |
| 9 | 75° | 48 | $<10^{-4}$ | Yes |

1) Statistical computation of direction and degree of preferred orientation and test of statistical significance of results have been done by the method presented by Curray (1956). As the final criterion for the significance of preferred orientations has been used the Rayleigh test of significance.

2) Angle measured clockwise from the foliation surface (s) to preferred orientation vetor on Plate 34-1.

3) Vector is accepted as significant if probability is $<0.05$.

* In analysis of the dimensional fabric in sectors 2, 3 and 8, the foliation surfaces are unfolded.

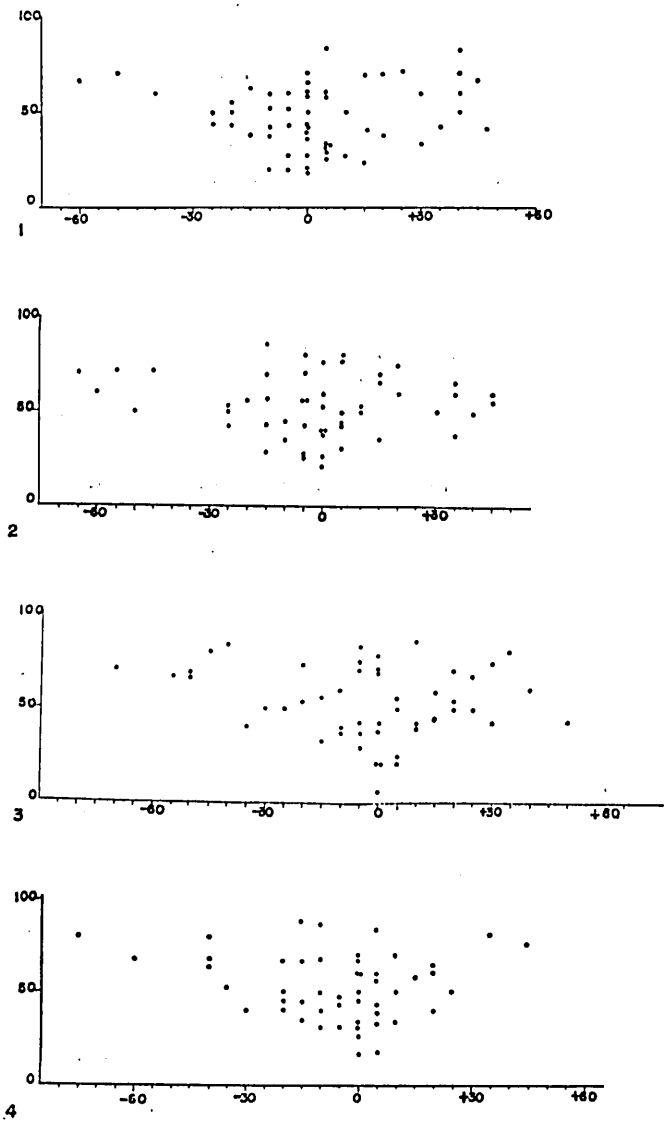


FIG. 2 The dimensional fabric of quartz grains in sectors 1 to 9 on Plate 34-2.

the ordinates: $\underset{(X)}{\frac{100}{X}} = \frac{\text{the longest dimension}}{\text{dimension normal to the longest dimension}}$

the abscissas: the angle between the elongation axis of grain and foliation surface (S).

Angle measured clockwise from the foliation surface to the elongation axis of grain on Plate 34-1.

In the diagrams for sectors 2, 3 and 8 the foliation surfaces are unfolded.

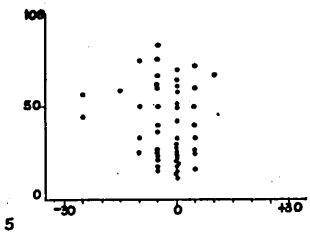
100
50
0
-30
0
+30

5

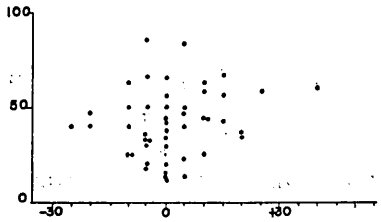
100
50
0
-30
0
+30

6

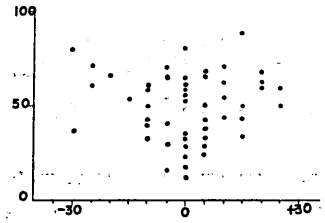
100
50
0
-30
0
+30

7

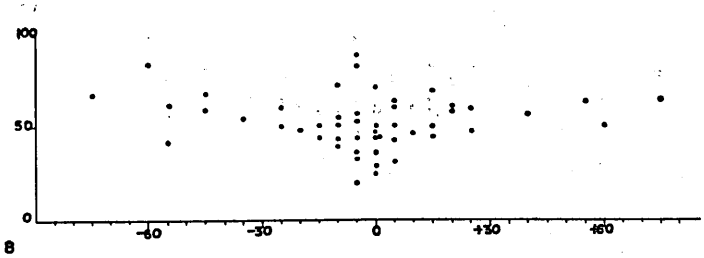
100
50
0
-60
-30
0
+30
+60

8

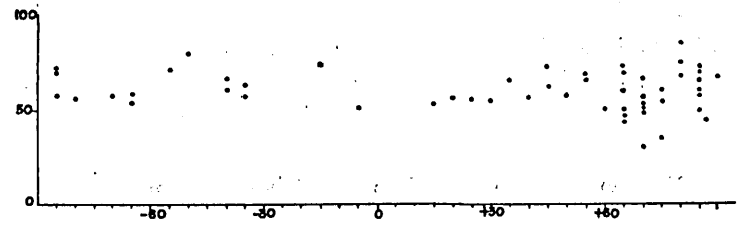
100
50
0
-60
-30
0
+30
+60

9

consisting of minute dark materials and minute flaky mineral grains, that traverse the layer j at high angles. The planar structures are displayed under high magnification as a crimpy surface running along the grain boundaries of quartz on the ac thin section (Plates 36-3 and 4, 37-5 and 6, 38-1, 2 and 3 and 39-1, 2, 3 and 4). They seem to be subparallel to the fold-axis as a whole. Transposition of the quartz-rich layer j along the surfaces in question can not be detected. The transversal surfaces will be regarded as a tension fracture filled with minute dark materials and minute flaky mineral grains (probably referred to the type of intercrystalline fracture). They correspond to the F-surface in Plate 34-1.

The quartz c-axis fabric of Fq zones 1 to 10 is illustrated in Fig. 4. It can be classified into the following two types: 1) The first type of the c-axis fabric is represented by Fq zone 8 (Fig. 4-h). It is characterized by a weakly defined great circle girdle, though it is broken near the pole of foliation surface. The diagram shows approximately a monoclinic symmetry whose symmetry plane coincides with the great circle girdle. The symmetry axis, the fabric axis b, normal to the girdle coincides with the fabric axis b for the mica fabric parallel to the fold-axis. 2) The second type comprises Fq zones 1 to 7 and Fq zones 9 and 10 (Fig. 4-a to g and i and j). In the diagrams for these zones the c-axes of quartz demonstrate random orientation.

Fig. 5 is a collective diagram for Fig. 4-a to g made of the fold in the present form. Fig. 6 is a collective diagram for the c-axis fabric of the Fq zones occurring in the left limb of the fold, whose trends in the diagram are parallel to one another. In both diagrams orientation of the c-axes is random.

Plate 37-3 is a photo of Fq zone 8 on the ac thin section. It shows evidence of shear movement along the zone. The sense of shear movement is parallel to that on the surface of décollement along the axial plane of fold C. Quartz grains in this zone does not demonstrate any significant fracturing and granulation as well as quartz grains of the host quartz-rich layers. Therefore, it is clear that the shear movement along the zone occurred by paracrystalline grain deformation. On the other hand, other Fq zones, except Fq zones 9 for which displacement of small magnitude is detected (Plate 37-1 and 2), present no evidence of shear movement along them (*e. g.* Plate 35-1). The sense of displacement along Fq zone 9 is the same as that along Fq zone 8.

The quartz c-axis fabric in the host quartz-rich layers was examined in 9 sectors in Plate 34-2 and shown in Fig. 7. Generally, all the diagrams show approximately monoclinic symmetry and the symmetry axis of them, the fabric axis b, all coincides practically with the fold-axis. The pattern is not homogeneous through the fold. It may be roughly classified into two types as follows: 1) The first type of fabric pattern is of the c-axis fabric for sectors 4, 5, 6 and 7 which are placed on fold B. It is characterized by a sharply defined narrow ac great circle girdle normal to the fold-axis. Furthermore, in the diagrams, the c-axes of quartz tend to form a concentration at high angles to the foliation surface. 2) The second type comprises

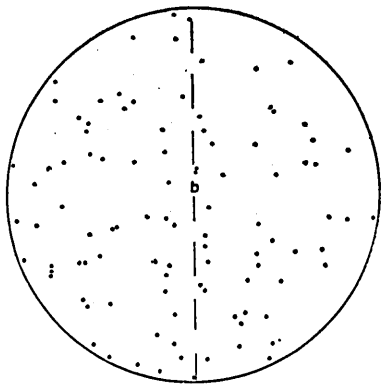


FIG. 3 The c-axis fabric of quartz grains of crossed part in Plate 34-1. broken line: the axial plane of fold A.

FIG. 4 The quartz c-axis fabric of the Eq zones 1(a), 2(b), 3(c), 4(d), 5(e), 6(f), 7(g), 8(h), 9(i) and 10(*j*). solid line (s): the foliation surface. broken line: the trend of Fq zone. a. p.: the axial plane of fold C.

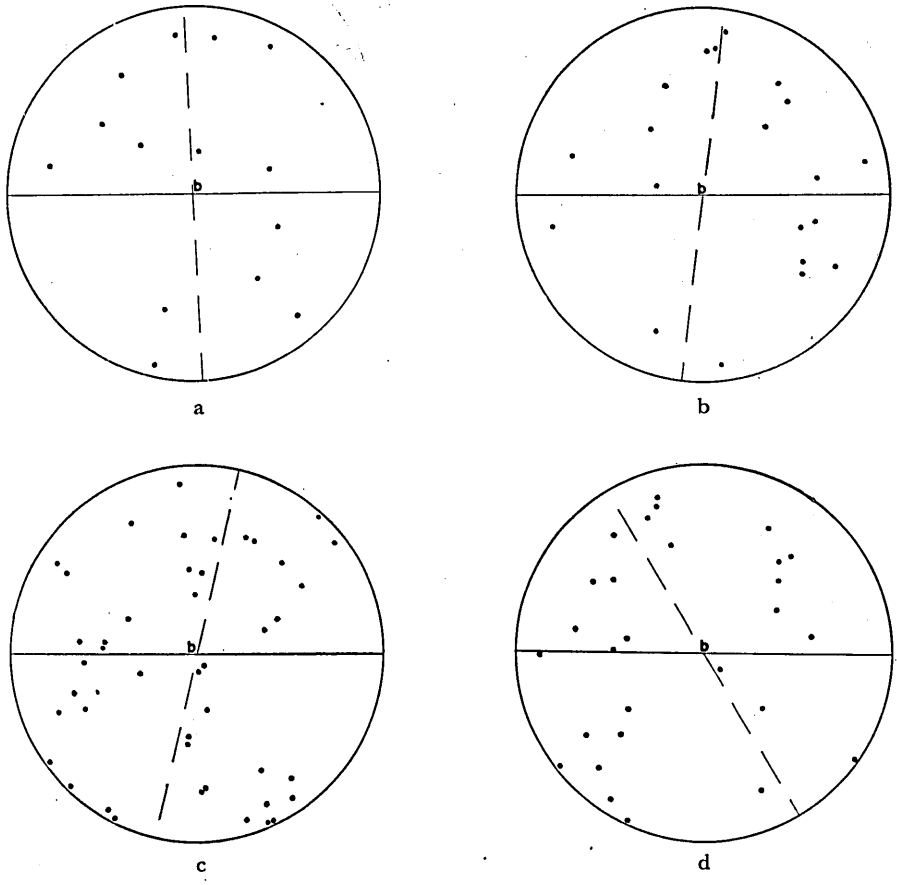

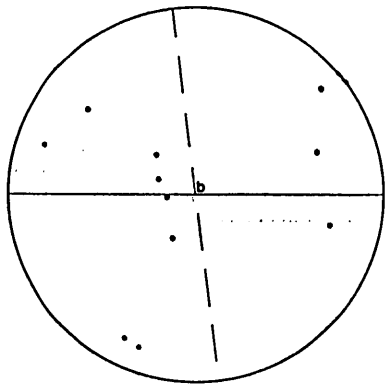


c

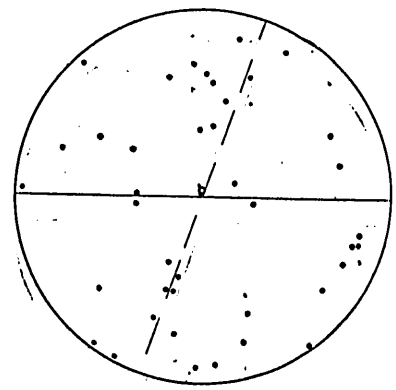


f

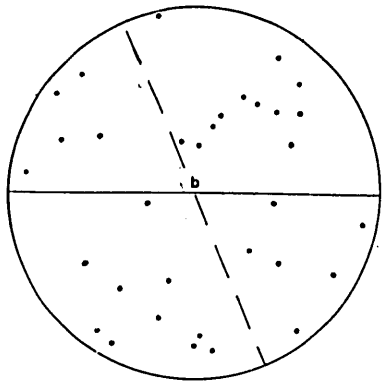


g

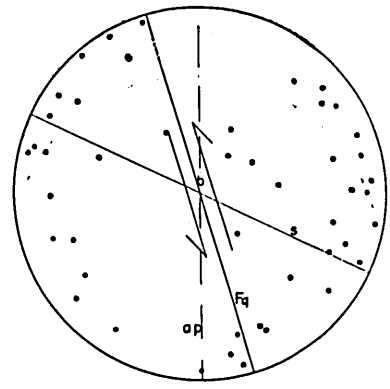


h

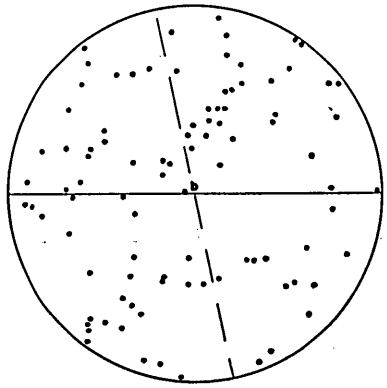


i

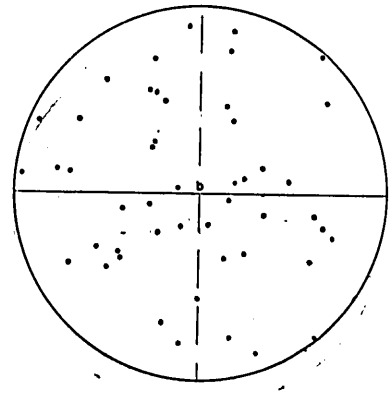


j

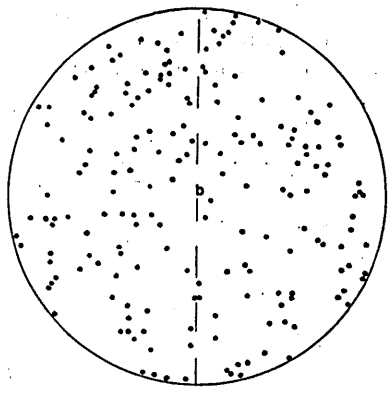

FIG. 5 Collective diagram for Fig. 4-a to g made for the fold in the present form. broken line: the axial plane of the fold.

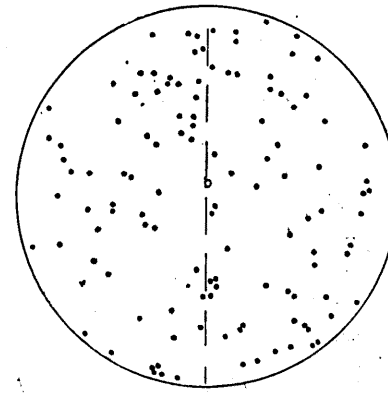

FIG. 6 Collective diagram for the quartz c-axis fabric of the Fq zones occurring in the left limb of the fold, whose trends in the diagram are parallel to one another. broken line: trend of the Fq zone.

the c-axis fabric of sectors 1, 2 and 3, which are placed on fold C, and that of sectors 8 and 9 which are placed on fold A. In the diagrams many of c-axes of quartz tend to be situated away from the ac great circle. The pattern can be termed "ac cleft girdle", and angular radius of the small circle girdle is approximately 70°. Therefore, we can point out a similarity between fold A and fold C and a discrepancy between fold B and folds A and C also with reference to the pattern of the quartz c-axis fabric.

The lamellar structures which will be examined in the later pages are found in quartz grains of both Fq zones and host quartz-rich layers. It is clear that the processes related to the formation of the Fq zones took place after the deformation related to the lattice and dimensional fabrics of quartz grains of the host quartz-rich layers and before the deformation related to the formation of the lamellar structures. However, we can not directly determine the time-relation between the Fq zones and the F-surfaces and that between the F-surfaces and the lamellar structures under the optic microscope*. Along the axial plane of the fold a fracture plane which is

* The mechanism that explains the time-relation of these surfaces, including Fq zones, may be explained as follows. In the later stage of the deformation related to the formation of the lattice and dimensional fabrics of quartz grains of the quartz-rich layers, these layers were deformed with formation of tension fractures in some parts of the fold. Then, these fractures were filled with $SiO_2$-precipitating solution which would have flowed through the host layer. As the tension fractures must represent the portions of pressure minima, quartz grain growing there has lower free energy than that in the compact host quartz-rich layers (cf. H. RAMBERG, 1952). Consequently, in those fractures quartz grains crystallized newly from the $SiO_2$ precipitating solution, accompnied by recrystallization (coarsening) of quartz grains at the walls of the fractures. The Fq zones in question may be regarded as the tension fractures filled with crystallized and recrystallized quartz grains. In the course of time, magnitude of flow of $SiO_2$-precipitating solution through the quartz-rich layers, that is, the indirect componental movement in the system concerned, suddenly decreased and became insignificant. Fq zone 10 consisting of fine granular grains of quartz may represent the structure of this stage, and the F-surfaces may be a structure formed at a stage slightly later than the former. The change of texture from Fq zones 1 to 9, through Fq zone

FIG. 7 The c-axis fabric of quartz grains of the host quartz-rich layers examined in sector 1(a), 2(b), 3(c), 4(d), 5(e), 6(f), 7(g), 8(h) and 9(i). solid lines: the foliation surface. broken line: the axial plane of fold A or fold C. Contours: 7-6-5-4-3-2-1%

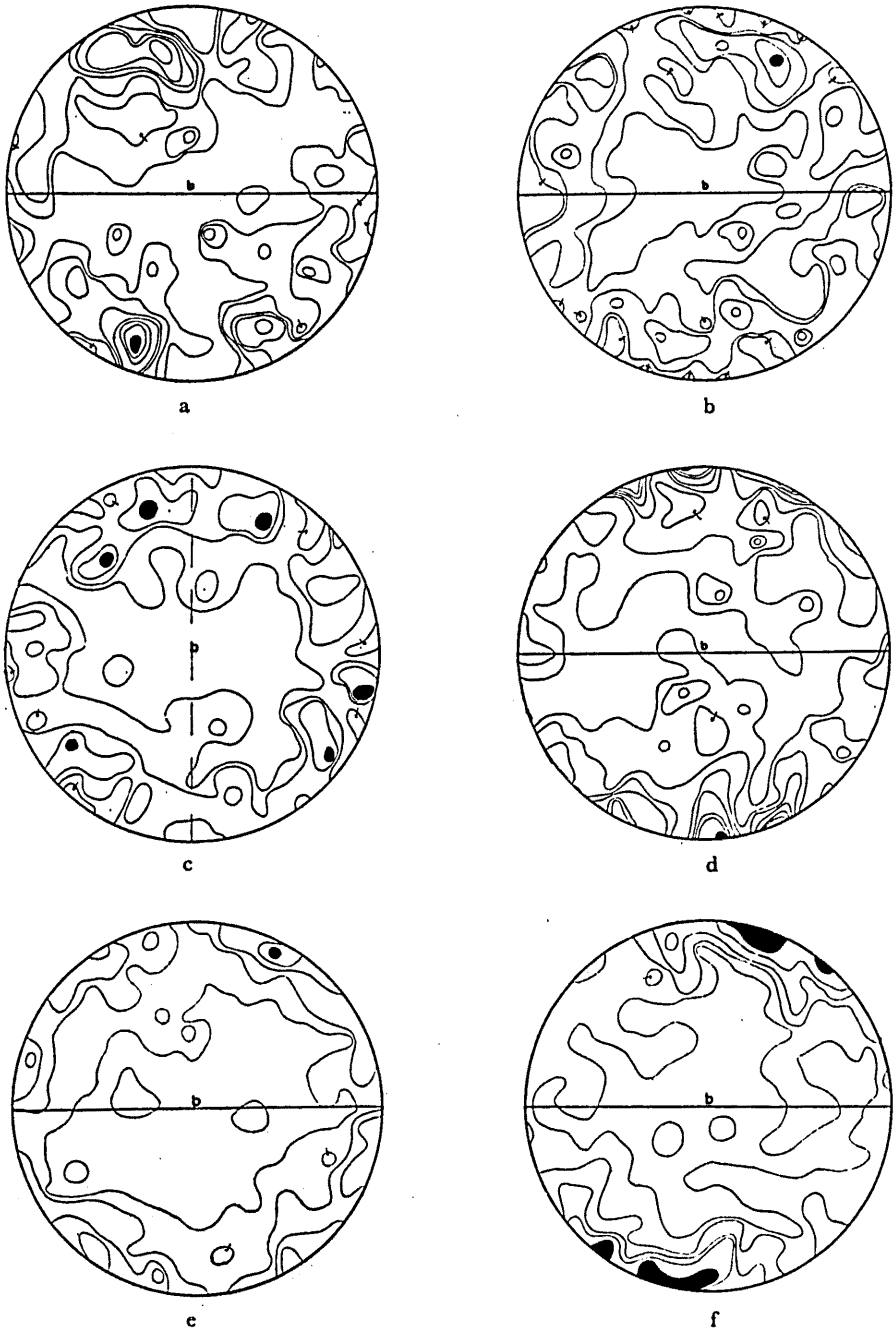

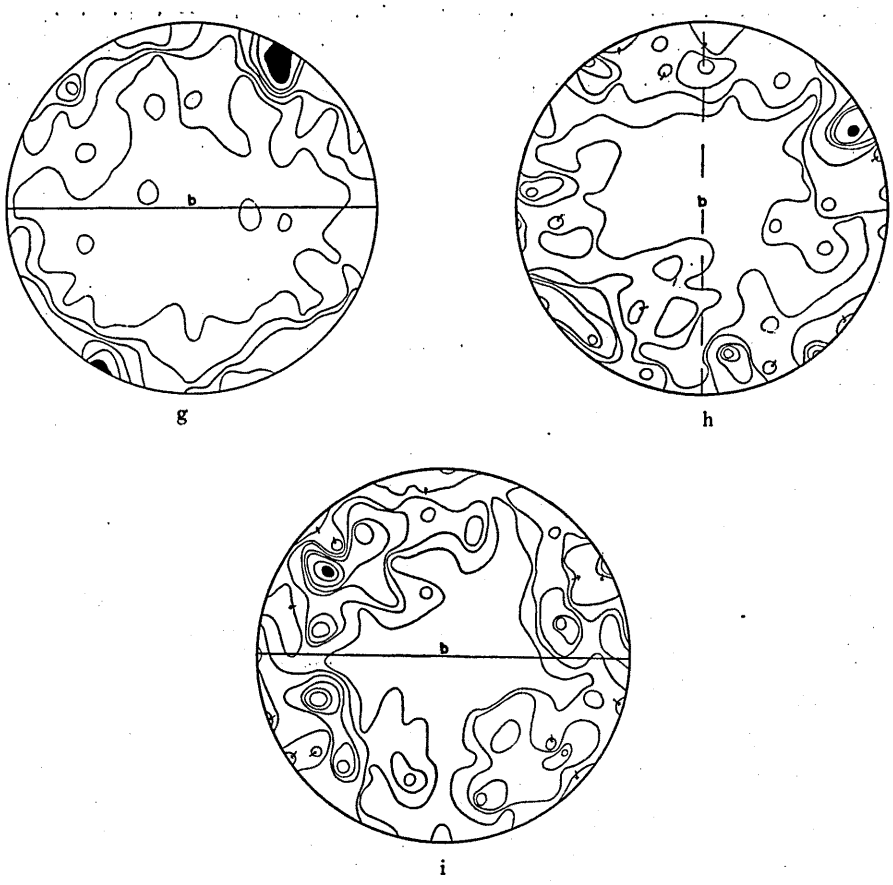


10, to the F-surfaces corresponds to the retrogressive change of metamorphic condition (especially temperature) in the system concerned.

Fractures formed initialy in quartz aggregate (the quartz-rich layers) related to the formation of the Fq zones might have been an intercrystalline fracture as referred to the F-surface. In other words, the deformation of quartz aggregate related to the formation of fractures for the Fq zones might have been caused by fracturing along the grain boundaries. The deformation related to the formation of the Fq zones was followed by what produced the lamellar structures and transcrystalline fractures in quartz grains of those zones and the host quartz-rich layers. It is not clear whether the temperature in the system concerned was higher during the stage of the former than during the stage of the latter or not. CONRAD says in the case of metal, "At low and intermediate temperature the deformation of a polycrystalline metal occurs essentially by deformation of the grains, and the fracture is transcrystalline. As the temperature is increased above approximately 0.5 Tm, significant sliding occurs along the grain boundaries and the fracture is generally intergranular with a marked reduction in ductility. ····· The temperature at which the fracture changes from transcrystalline to intergranular depends on the strain rate. ····· the temperature at which a reduction in ductility occurs decreases as the rate of straining is decreased." (H. CONRAD, 1961). It may be said that analogous relationship is also valid for the metamorphic deformation of quartz aggregate, though possiblly with some reservations. However, this problem is beyond the scope of this paper, and the specimen in question is not adequate to give data effective for the discussion of the problem.

planar and open is found, as shown in Plates 34-1 and 40-4. Probably it is referred to the type of the tension fracture. It is a structure of the latest stage observed in the fold. The fracture is running through the quartz aggregate in a fashion of transcrystalline fracture.

## III. Analysis of Lamellar Structures in Quartz

Two types of lamellar structures have been recognized in quartz grains of the Fq zones and the host quartz-rich layers. One type of the lamellar structure is defined by the closely spaced planar structure consisting of minute dark inclusions, terminating within the grain boundaries (Plate 40-1 and 2). Namely, the lamellae of this type correspond to the Böhm lamellae. The second type of the lamellar structure is distinctly displayed as narrow bands of different lattice orientation across the host crystal, terminating within the grain boundaries (Plate 40-2 and 3). In each of the grains containing the lamellae of this type the change in lattice orientation from band to host crystal is in the same rotational sense. Namely, they correspond to deformation bands after RILEY (1947) and to the lamellae noticed previously as the lamellae of Type L3 by the present author (1961b and 1963).

Coexistence of the Böhm lamellae and deformation bands in the same grain has been recognized in 10 quartz grains. The former and the latter, when they occur in the same grain, are either parallel or oblique to each other on the plane of thin section normal to the fold-axis (Fig. 26-a and b). We can not determine time-relation between the Böhm lamellae and deformation bands under the optic microscope (*e. g.* Plate 7-2). CARTER *et al.* (1961) and CHRISTIE *et al.* (1962) said, on the basis of experimental deformation of quartz sand and quartz single crystal, that the formation of the Böhm lamellae was associated with deformation bands or undulatory extinction. It is not clear whether the deformation bands experimentally formed are identical with those in the present specimen (and also in other specimens previously described by the present author) or not.

The lamellae of any type have not been recognized in quartz grains sporadically occurring in the mica-rich layers.

### A. Deformation Bands

The crystallographic location of the deformation bands, displayed as narrow bands of different lattice orientation across the host crystal, can not be accurately measured with the U-stage and only their trend on the plane of thin section can be directly determined. Therefore, also the width of each of the deformation bands and the spacing between them can not be directly measured. At present we can measure only their apparent width and spacing on each thin section, as in the previous cases (HARA, 1961b and 1963). Some boundaries between the band and host crystal are displayed as sharp but continuous changes in extinction position, and others as

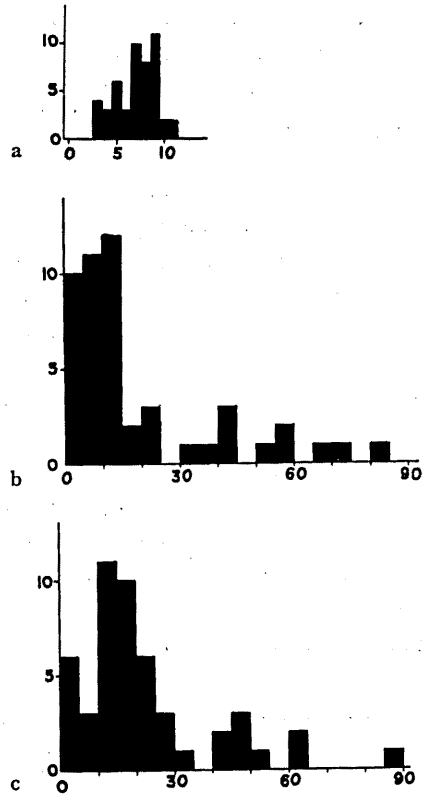


FIG. 8 a) Histogram showing the variation in the angle between the c-axis of host crystal and that of band crystal for the deformation bands in subareas A to G.
b). Histogram showing the variation in the angle between the c-axis of band crystal and the pole of deformation band for the deformation bands in subareas A to G.
c) Histogram showing the variation in the angle between the c-axis of host crystal and the pole of deformation band for the deformation bands in subareas A to G.

discontinuous changes. The apparent width of the bands on the plane of thin section normal to the fold-axis is less than 0.012 mm, that being similar to the result noticed previously by the author (1963). The apparent spacing in question is 0.006 to 0.027 mm, that being similar to the result for the Böhm lamellae described in the later pages.

The relative potitions between the c-axis of the deformation band ($C_L$) and that of the host crystal (Ch) could be measured in all of the grains containing the deformation bands. The value of shift in the c-axis from the host to band ($Ch \wedge C_L$) in measured grains is between 3° and 11°, with a maximum between 7° and 9°, as shown in Fig. 8-a. This result is quite similar to that of the specimens examined previously by the author.

From the X-ray studies of quartz grains exhibiting deformation features including undulatory extinction, deformation lamellae, marginal granulation and fracturing in naturally deformed rocks, BAILEY *et al.* (1958) said, "... most of the quartz has deformed plastically by bend gliding. One of the three crystallographic a axes is always the major axis of bending, ..." On the other hand, HERITSCH *et al.* (1954) concluded, "Die Laueaufnahme ... zeight Asterismus, der als *axis of bending* die Kante m:c besitzt" in addition to the a-axis, on the X-ray studies of quartz grains exhibiting undulatory extinction. On those bases, it will be expected that for the deforma-

tion bands in question generally the rotational axis of shift in the c-axis from band to host crystal coincides with either the a-axis or the a*-axis. Therefore, the crystallographic location of the deformation bands in question has been tentatively determined on the basis of assumption that the rotational axis of shift from Ch to CL coincides with either the a-axis or the a*-axis.

The crystallographic location of the deformation bands in question was examined by measuring angles between Ch and L⊥ and between CL and L⊥, respectively (Fig. 8-c and b). The angle between Ch and L⊥ (Ch∧L⊥) is between 1° and 89°, showing a wide range of the crystallographic location of the deformation bands. For many grains, however, Ch∧L⊥ is between 1° and 22°, which is similar to the results previously noticed by the author and further to the results for the Böhm lamellae noticed by SANDER (1930), FAIRBAIRN (1941), INGERSON and TUTTLE (1945), HANSEN and BORG (1962) and HARA (1963). The angle between CL and L⊥ (Cl∧L⊥) is between 1° and 83°, with a strong maximum between 1° and 15°.

Plate 34-3 shows the distribution of quartz grains containing the deformation bands through the fold and the trend of the bands in each grain, analysed on the thin section normal to the fold-axis. Most of the grains are distributed in two sharply restricted parts in the fold, that is, in the knee of layer j and a part of the right limb of fold C (the knee of fold C'). All these parts correspond to the "knee of fold."

The orientation of poles of the deformation bands assumed is illustrated in Fig. 9. It is characterized by an incomplete great circle girdle normal to the fold-axis, indicating that the deformation bands are roughly tautozonally oriented with respect to the fold-axis. The pattern of the L⊥ diagram shows a monoclinic symmetry with a single symmetry plane normal to the fold-axis. Although the variation in the trend of deformation bands in question is represented as an incomplete great circle girdle in the L⊥ diagram, they do not run at random through the fold, but they seem to change their trend regularly in connection with the change of position on the fold, as read in Plate 34-3.

Areas where the deformation bands and the Böhm lamellae have been recognized were divided into 8 subareas, that is, subareas A to H in Plate 34-2, with reference to pattern of the composite diagram for Ch, CL and L⊥ which will be examined in the later pages. Most of grains containing the deformation bands have been recognized in subareas A to F. In Figs. 10 to 14 we can examine the trend of the deformation bands in those subareas respectively.

The deformation bands in subarea A have their poles distributed in two restricted parts in the diagram (Fig. 10), centers of which lie with an angular distance ca. 90° in the fabric plane ac for the mica fabric, this fact indicating that they correspond approximately to two sets of (h01)-planes with reference to the fabric axes for the mica fabric. The L⊥ diagram shows monoclinic symmetry with a single symmetry plane normal to the axis coinciding with the fabric axis b for the mica fabric (the fold-axis). Therefore, it can be pointed out that the latter is identical with the fabric

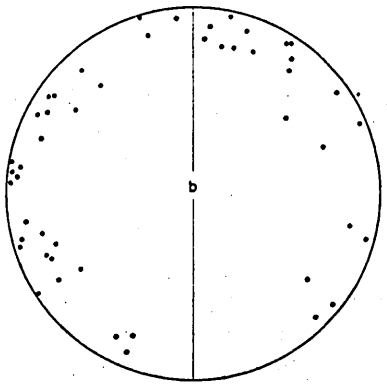


FIG. 9 Poles of the deformation bands in subareas A to G. solid line: the axial plane of the fold.

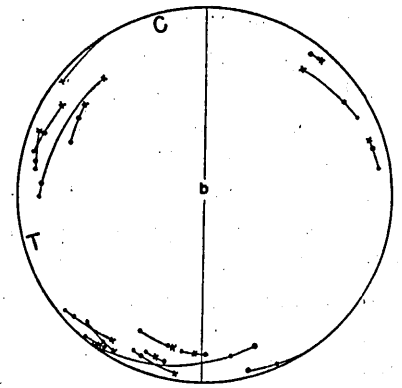


FIG. 10 Poles of the deformation bands (crosses) and c-axes of band (circles) and of host crystals (dots) in 16 grains in subarea A. solid line: the axial plane of the fold C'.

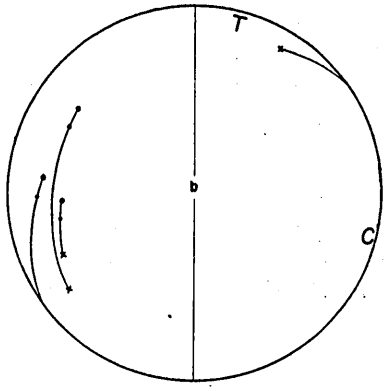


FIG. 11 Poles of the deformation bands (crosses) and c-axes of band (circles) and of host crystals (dots) in 3 grains in subarea B. solid line: the axial plane of the fold C.

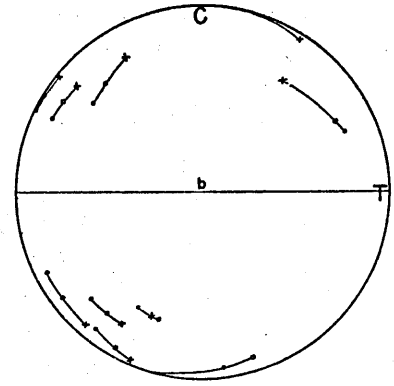


FIG. 12 Poles of the deformation bands (crosses) and c-axes of band (circles) and of host crystals (dots) in 9 grains in subarea C. solid line: the foliation surface.

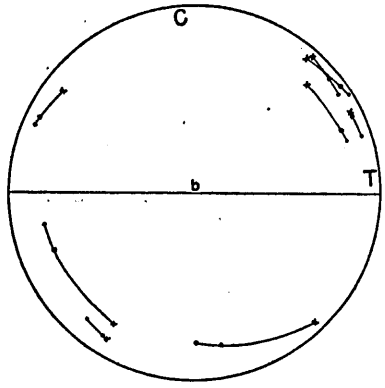


FIG. 13 Poles of the deformation bands (crosses) and c-axes of band (circles) and of host crystals (dots) in 8 grains in subarea D. solid line: the foliation surface.

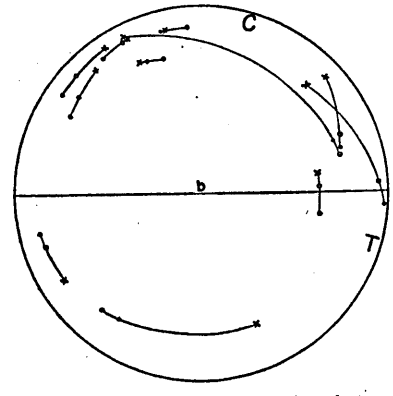


FIG. 14 Poles of the deformation bands (crosses) and c-axes of band (circles) and of host crystals (dots) in 11 grains in subareas E and F. solid line: the foliation surface.

axis b for the deformation band fabric in subarea A. Analogous pattern of the deformation band fabric is equally obvious for subareas C, D, E and F, as read in Figs. 12 to 14. Fig. 11 for the deformation bands in subarea B represents that they correspond approximately to one set of (h01)-planes with reference to the fabric axes for the mica fabric. Thus, it can be generally said that the fabric axis b for the deformation band fabric is parallel to that for the mica fabric.

As mentioned in the preceding page, for the deformation bands the rotational axis of shift in the c-axis from the host crystal to band was assumed to coincide with either the a-axis or the a*-axis, according to the X-ray studies of naturally deformed quartz grains after BAILEY *et al.* and HERITSCH *et al.*. In Figs. 10 to 14, generally, the great circles containing Ch and CL are parallel or subparallel to the ac great circle. This fact indicates that the b-kinematic axis in the deformation related to the deformation bands was parallel to the fold-axis throughout the quartz aggregate (quartz-rich layers) concerned.

Previously the author demonstrated that the deformation bands are oriented with an angle ca. 45° to the direction of the principal normal stresses in the system concerned, and that the rotational sense of the changes in lattice orientation from the host to the band crystal is reversed when compared with gliding on any active glide plane induced in any grain under the stress system. On this basis, he concluded that the deformation bands in question are correlated with one of deformation bands inclined at high angles to the active glide line usually demonstrated by experimental studies of metals, and that A. H. SULLY's terms (1956) about the formation of kink or deformation bands in creep deformation of polycrystalline metalic aggregates—— "as slip proceeds, local stress concentrations are set up inside individual crystals, due to the intersection of slip with the grain boundaries and the constraining effect of neighbouring grains. These stress concentration may be relieved by local distortions of the crystals which take place the form of kink or deformation bands" —— would be also valid for the formation of the deformation bands in quartz grains. The relationship between Ch, CL and L⊥ in the Ch-CL-L⊥ diagrams (Figs. 10 to 14) for the deformation bands in the present specimen is essentially the same as that in the specimens previously described by the author.

The author (1961a and 1963) proposed a rule for establishing the stress system (only the direction of the principal stresses) in the deformation related to the deformation bands in the system concerned. According to the rule, points C and T in Figs. 10 to 14 correspond to the direction of the principal compressive stress and that of the principal tensile stress respectively. In subarea A the principal compressive stress is directed approximately parallel to the axial plane of fold C′ and normal to the fold-axis. In subarea B the principal compressive stress is directed subnormal to the axial plane of fold C. From Figs. 12 to 14, it can be generally said that the principal compressive stress is approximately directed normal to the foliation surface in any position of the fold of layer j and that the principal tensile stress is approximately directed parallel to the foliation surface and normal to the fold-axis.

Another intracrystalline deformation structure observed in quartz grains, which formed contemporaneously with the deformation bands, is undulatory extinction. Generally, it occurs in broad bands between which the change in orientation of the c-axis appears to be gradual or sudden under the microscope. In grains containing the deformation bands, generally, bands of undulatory extinction are inclined at high angles to the former on the thin section normal to the fold-axis. While in grains lacking the deformation bands the undulatory extinction bands seems to be parallel or subparallel to the c-axis. As read in Plate 34-3, the grains containing the deformation bands are distributed in two sharply restricted parts in the fold, while the grains exhibiting the undulatory extinction are found all over the fold.

On the basis of the above descriptions and considerations, the right limb of fold C (fold C′) can be divided into three domains with reference to deformation style of quartz grains in the stage of the deformation related to the formation of the deformation bands as follows (Fig. 15-a): domains 1 and I′ where quartz grains were deformed in such a manner as only the undulatory extinction was induced in many of them, and domain II where quartz grains were deformed in such a manner as the deformation bands were formed in some of them and the undulatory extinction in many of them. The pattern of the Ch-CL-L⊥ diagram indicates that the movement picture in the deformation related to the deformation bands was statistically homogeneous within domain II. As read in Fig. 15-a, the arrangement of these domains on either side of the axial plane of fold C′ are approximately symmetrical.

The fold of layer j can be divided into three domains with reference to deformation style of quartz grains in the stage of the deformation related to the formation of the deformation bands as follows (Fig. 15-b): domains I and I′ where quartz grains were deformed in such a manner as only the undulatory extinction was formed in many of them, and domain II where quartz grains were deformed in such a manner as the deformation bands were formed in some of them and the undulatory extinction in many of them. Domain II can be divided into three homogeneous subdomains with reference to the movement picture in the deformation related to the deformation bands, that is, subdomain II′ corresponding to subarea C (Fig. 12), subdomain II″ to subarea D (Fig. 13) and subdomain II‴ to subareas E and F (Fig. 14). As read in Fig. 15-b, the arrangement of these domains and subdomains on either side of the axial plane of the fold of layer j are approximately symmetrical. If two grains containing the deformation bands in subarea G are considered as significant, Fig. 15-b (only for the layer j) will be modified into Fig. 15-c.

Now we will consider why most of the deformation bands are found in two restricted parts of the fold (domain II of the fold of layer j and of fold C′), which all correspond to the "knee of fold". If mechanism of the formation of the deformation bands is to be explained in SULLY's terms cited in the preceding page, it seems most reasonable to answer this question as follows: For individual quartz grains in domains I and I′ of the fold of layer j and fold C′, the constraining effect of neighbouring grains in the process of deformation was insignificant, and consequently no deforma-

tion bands were induced in any grain, but only broad undulatory extinction bands were weakly induced in many grains of quartz. On the other hand, the restriction on some grains of quartz in domain II was so intensive, that in those quartz grains the deformation bands were produced. Then, one might assume that degree of the restriction on individual grains in question is approximately proportional to the magnitude of the mean pure strain of quartz aggregate in those domains, and so that the above-described discrepany between domain II and domains I and I′ corresponds approximately to that with respect to the magnitude of the mean pure strain of quartz aggregate between these domains. On this basis, one supposes that during the deformation related to the formation of the deformation bands, post-crystalline folding of the quartz-rich layers, the mean pure strain of quartz aggregate (quartz-rich layer) in domain II (knee of fold) was greater than that in domains I and I′ (limbs of fold), and so that the principal normal stresses (corresponding to the strain in question) were greater in domain II than in domains I and I′. However, "during plastic or viscous buckling of a sheet of homogeneous nonstratified rock, longitudinal as well as shearing strain occur parallel to the folded surface and perpendicular to the fold axis. One may refer to these strains as the concentric strains. Concentric longitudinal strain predominates in the crest of the folds where curvature is greatest, being compressive on the concave side of the neutral middle surface and extensive on the convex side. Concentric shearing strain predominates along the flank of the folds where curvature is at minimum." (RAMBERG, 1961). Analogous relationship of the strain of rock might have been also developed in the present case, post-crystalline folding of quartz-rich layers (multiple-layered system), and such a discrepancy between the knee and limbs in relation to kinds of strain might have been responsible for that between domain II and domains I and I′ in relation to the movement picture.

On what causes does it depend that quartz grains containing the deformation bands are not found in the quartz-rich layers of the left limb of fold C and in the quartz-rich layers l, n, p and r involved in fold B? As shown in Plate 34-1, displacement on the surface of décollement along the axial plane of fold C took place in such a manner as the right side of fold C was slid up relatively to the left side, though not so obstinct. It is not determined whether the displacement in question took place during the deformation related to the deformation bands or not. If these two types of deformation occurred simultaneously, however, movement of the layers involved in fold C would have occurred from the right to the left on Plate 34-1. In this manner will be reasonally explained the fact that quartz grains containing the deformation bands are not found in the left limb of fold C, but that they occur only in domain II of the right limb (knee of fold C′). On the other hand, the problem why quartz grains containing the deformation bands are not found in the quartz-rich layers l, n, p and r involved in fold B, while in the quartz-rich layer j involved in fold B the deformation bands are found in fairly number of quartz grains, is also not so readily explained, but it may be said that the presence of row of voids in the

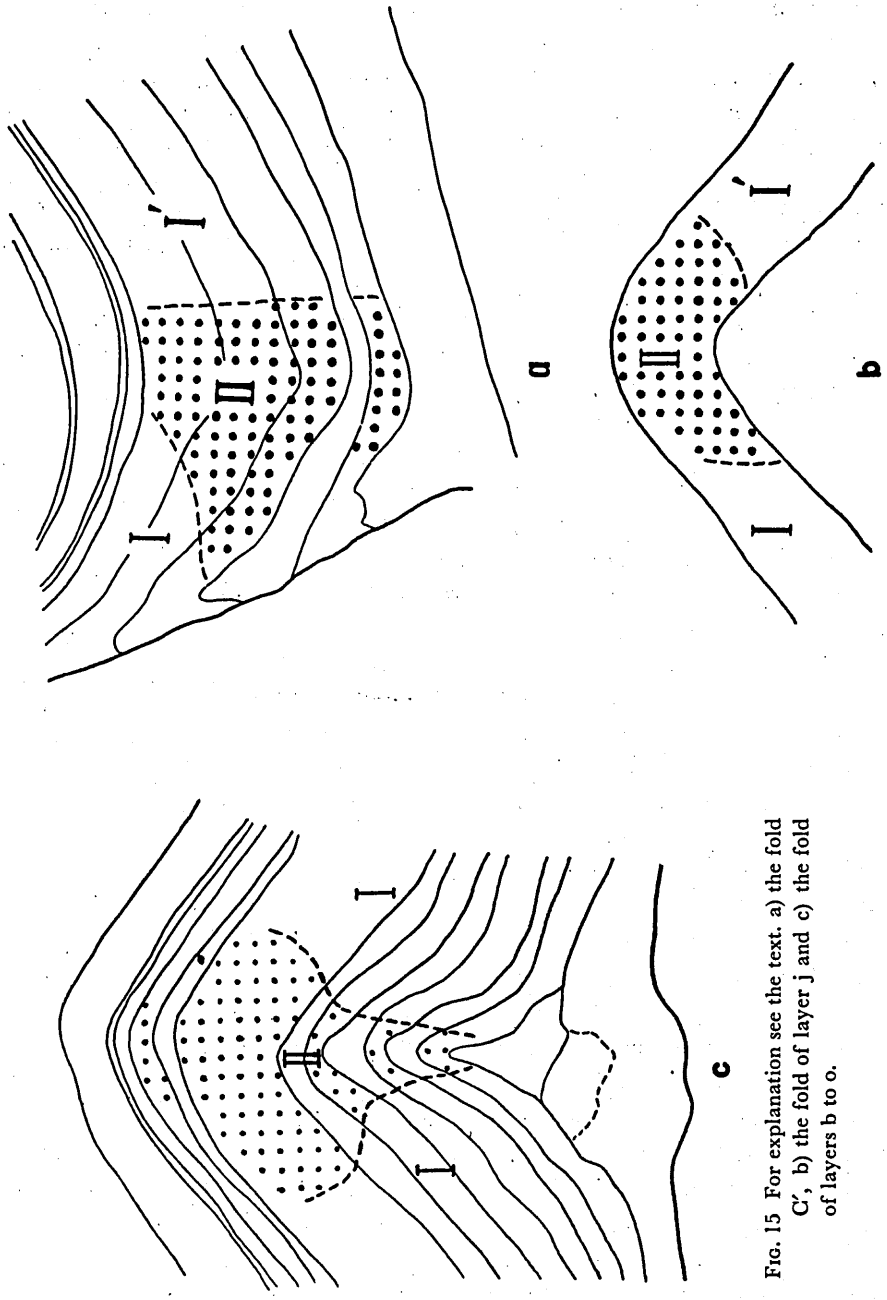


FIG. 15 For explanation see the text. a) the fold C', b) the fold of layer j and c) the fold of layers b to o.

Fq zone 9 which cut across the layers l, n, p and r, but not across the layer j, must be noticed in this connection.

### B. Böhm Lamellae

The Böhm lamellae could be measured on the U-stage by tilting them untile they became parallel to the axis of the microscope. The width of each of the Böhm lamellae is less than 0.009 mm, and the spacing between them is approximately 0.005 mm to 0.022 mm, that being similar to the results of RILEY (1947) and HANSEN *et al.* (1962).

The crystallographic location of the Böhm lamellae was examined by the measurement of angles between Ch and L⊥. Ch∧L⊥ is between 2° and 89°, that showing large variation of the crystallographic location of the lamellae (Fig. 16-a). For many grains, however, Ch∧L⊥ is between 2° and 30°. This result is similar to that noticed by SANDER (1930), FAIRBAIRN (1941), INGERSON and TUTTLE (1945) and HANSEN and BORG (1962).

Plate 34-4 shows the distribution of quartz grains containing the lamellae through the fold and the trend of the lamellae in each grain, analysed on the thin section normal to the fold-axis. They are distributed in sharply restricted parts in the fold, that is, in the knee of fold A, the layer j and a part of the right limb of fold C (knee of fold C′). The latter two are approximately identical with the areas where the grains containing the deformation bands have been found.

The preferred orientation of poles of the Böhm lamellae through the fold, analysed on the thin section normal to the fold-axis, is illustrated in Fig. 17. It is characterized by a sharply defined great circle girdle normal to the fold-axis, indicating that the lamellae are roughly tautozonally oriented with respect to the fold-axis. Broadly speaking, the L⊥ diagram shows a monoclinic symmetry with a single symmetry plane normal to the axis coinciding with the fold-axis. Although the variation in the trend of the lamellae is represented as a great circle girdle in the L⊥ diagram, they do not run at random through the fold, but they seem to change their trend regularly in connection with the change of position on the fold, as read in Plate 34-4. In Figs. 18 to 24 we can examine the trend of the lamellae in subareas A, C, D, E, F, G and H respectively.

For the lamellae in subarea A their poles are distributed in two restricted parts in the diagram (Fig. 18), centers of which lie with an angular distance ca. 90° in the fabric plane ac for the mica fabric, this fact indicating that they correspond approximately to two sets of (h01)-planes with reference to the fabric axes for the mica fabric. The L⊥ fabric shows a monoclinic symmetry with a single symmetry plane normal to the axis coinciding with the fabric axis b for the mica fabric (the fold-axis). Therefore, the symmetry axis is the fabric axis b for the lamella fabric in subarea A. Analogous pattern of the lamella fabric is equally obvious for subareas C, F and G, as shown in Figs. 19, 22 and 23. Fig. 20 for the lamellae in subarea D

represents that they correspond approximately to one set of (h01)-planes with reference to the fabric axes for the mica fabric. In Fig. 21 for the lamellae in subarea E their poles form a great circle girdle with a distinct break. The axis normal to the girdle coincides with the fabric axis b for the mica fabric. Therefore, it can be pointed out that for the lamella fabric in layer j (subareas C to F) the fabric axis b is parallel to that for the mica fabric. For the lamellae in subarea H their poles are

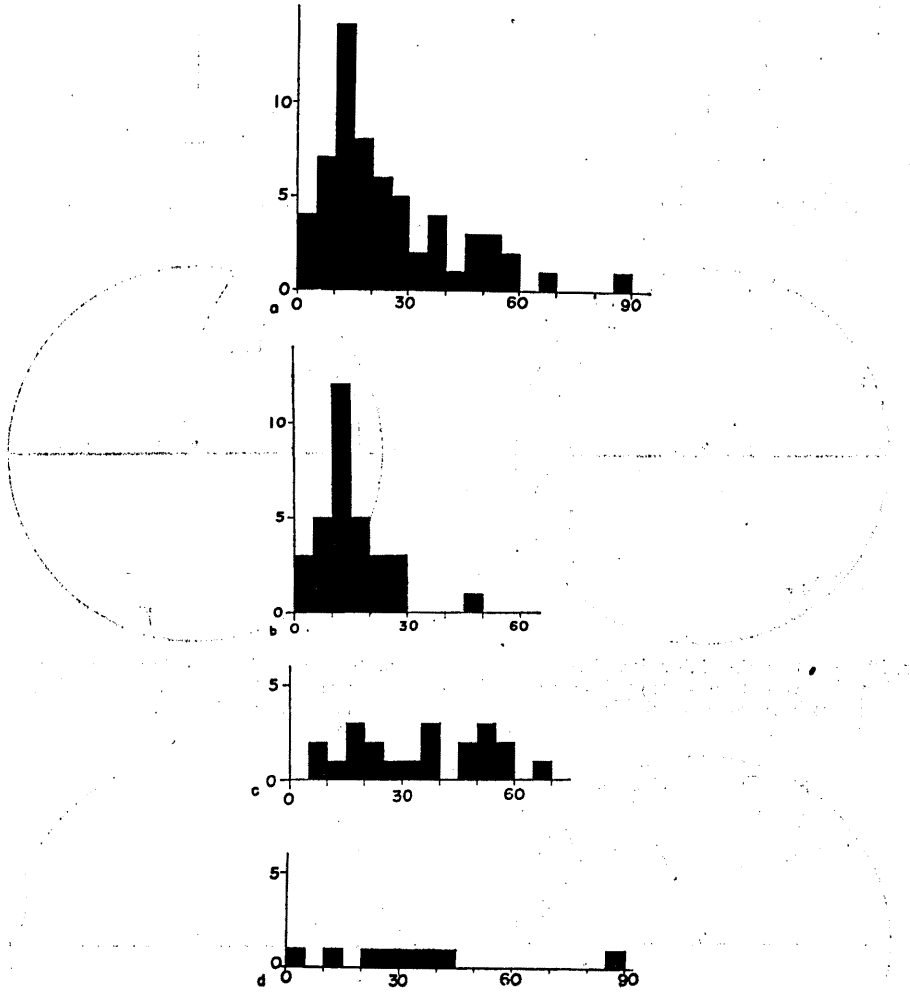


FIG. 16 a) Histogram showing the variation in the angle between the c-axis of host crystal and pole of lamellae for the Böhm lamellae in subareas A, C, D, E, F, G and H.
b) Histogram showing the variation in the angle between the c-axis of host crystal and pole of lamellae for the Böhm lamellae in subareas A, C, F and G.
c) Histogram showing the variation in the angle between the c-axis of host crystal and pole of lamellae for the Böhm lamellae in subareas D and E.
d) Histogram showing the variation in the angle between the c-axis of host crystal and pole of lamellae for the Böhm lamellae in subarea H.

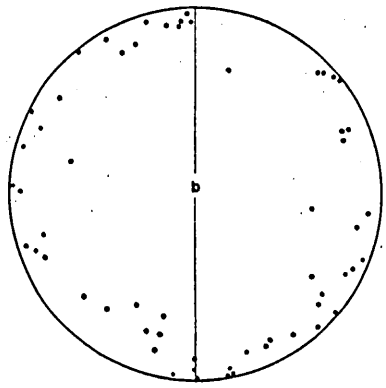


FIG. 17 Poles of the Böhm lamellae in subareas A, C, D, E, F, G and H. solid line: the axial plane of the fold.

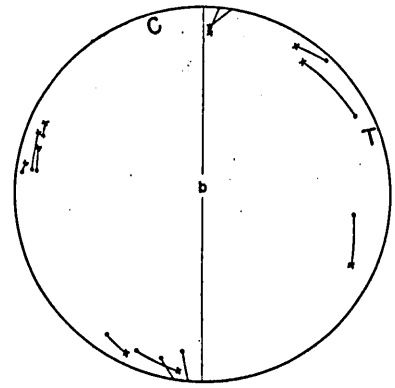


FIG. 18 Poles of the Böhm lamellae (crosses) and c-axes of host crystal (dots) in 11 grains in subarea A. solid line: the axial plane of fold C'.

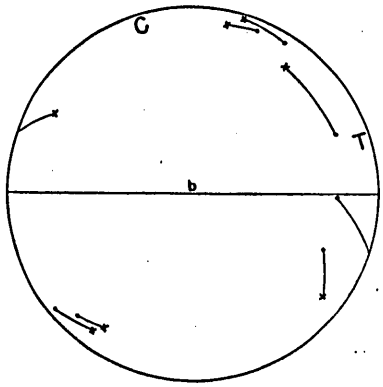


FIG. 19 Poles of the Böhm lamellae (crosses) and c-axes of host crystal (dots) in 7 grains in subarea C. solid line: the foliation surface.

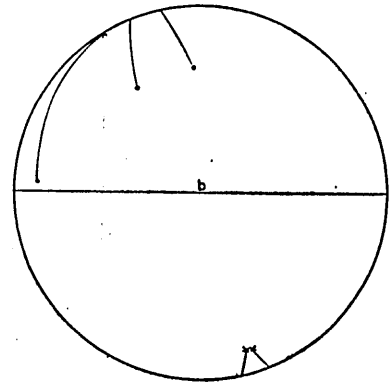


FIG. 20 Poles of the Böhm lbmellae (crosses) and c-axes of host crystal (dots) in 3 grains in subarea D. solid line: the foliatioo surface.

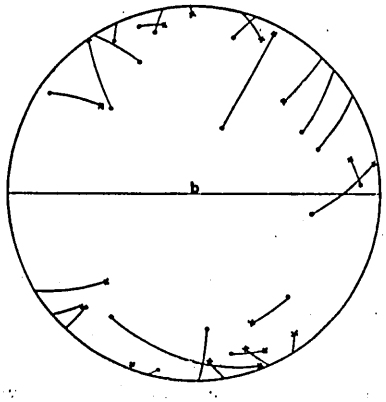


FIG. 21 Poles of the Böhm lamellae (crosses) and c-axes of host crystal (dots) in 17 grains in subarea E. solid line: the foliation surface.

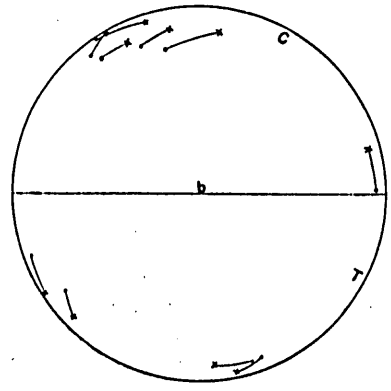


FIG. 22 Poles of the Böhm lamellae (crosses) and c-axes of host crystal (dots) in 10 grains in subarea F. soild line: the foliation surface.

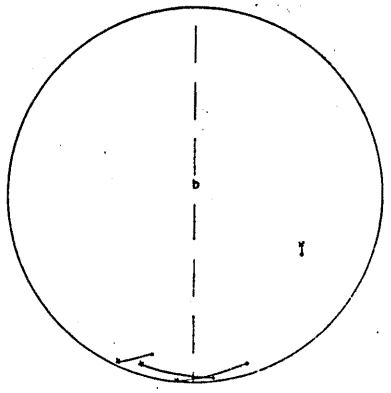


FIG. 23 Poles of the Böhm lamellae (crosses) and c-axes of host crystal (dots) in 4 grains in subarea G. broken line: the axial plane of fold A.

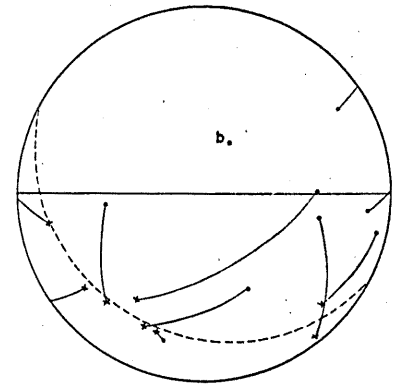


FIG. 24 Poles of the Böhm lamellae (crosses) and c-axes of host crystal (dots) in 8 grains in subarea H. solid line: the foliation surface.

distributed in two restricted parts in the diagram (Fig. 24), centers of which lie with an angular distance ca. 90° in the plane slightly oblique to the fabric plane ac for the mica fabric, and the pattern of the diagram shows a monoclinic symmetry. Two sets of planes of lamellae in this subarea are approximately symmetrically oriented to the axial plane of the fold of layer b, and the fabric axis b for the lamellae is slightly oblique to that for the mica fabric.

In Fig. 18, most of the great circles containing Ch and L⊥ are subnormal to the fabric axis b. Fig. 18 also represents a familiar regularity with respect to the positional relationship between Ch in any grain and L⊥ in the same grain, like in the specimens noticed by INGERSON and TUTTLE (1945), HANSEN and BORG (1962) and HARA (1963). Namely, in Fig. 18 L⊥ in any grain is closer to point C than Ch in the same grain. Points C and T lie together on the fabric plane ac containing two groups of the poles of lamellae distributed separately with an angular distance ca. 90°, and they lie midway between those two groups. In Fig. 19 for the lamellae in subarea C the great circles containing Ch and L⊥ are generally inclined at high angles to the fabric axis b. In the diagram we can find a regularity that L⊥ in any grain is closer to point C than Ch in the same grain. Analogous relationship between Ch, L⊥ and points C and T in the Ch–L⊥ diagram is equally obvious for subareas F and G, as read in Figs. 22 and 23. On the other hand, in the Ch–L⊥ diagrams for subareas D and E (Figs. 20 and 21), the great circles containing Ch and L⊥ demonstrate random orientation, inspite of marked preferred orientation of planes of the lamellae through those subareas. Moreover, we can not find any regularity with respect to the positional relationship between Ch and L⊥. Therefore, it can be concluded that the movement picture in the deformation related to the lamellae was of different types between subareas A, C, F and G and subareas D and E. In Fig. 24 for the lamellae in subarea H the great circles containing Ch and L⊥ tend to be inclined at moderate to high angles to the fabric axis b, rather like

in the case of the lamellae in subareas A, C, F and G. However, we can not find any regularity with respect to the positional relationship between Ch and L⊥, as in the case of the lamellae in subareas D and E.

Fig. 16-b is a histogram for the crystallographic location (Ch∧L⊥) of the lamellae in subareas A, C, F and G, for which the positional relationship between Ch and L⊥ in the Ch-L⊥ diagrams shows a distinct regularity. Ch∧L⊥ for the lamellae in those subareas is between 4° and 47°, with a strong maximum between 7° and 18°. This is quite similar to the result for the deformation bands described in the preceding pages. Fig. 16-c is a histogram for the crystallographic location of the lamellae in subareas D and E, for which in the Ch-L⊥ diagram no regularity can be detected. Ch∧L⊥ is between 9° and 66°, that showing large variation of the crystallographic location of the lamellae. The restriction in the crystallographic location of the lamellae in subareas D and E seems to be insignificant unlike the lamellae in subareas A, C, F and G. From these characteristics of the Böhm lamellae in subareas D and E, it seems probable that they, but probably not all, were formed by other mechanism than that for the Böhm lamellae in subareas A, C, F and G.

Fig. 16-d is a histogram for the crystallographic location of the lamellae in subarea H. Ch∧L⊥ is between 2° and 89°. The restriction in the crystallographic location of the lamellae seems to be insignificant, like the lamellae in subareas D and E. As mentioned in the preceding paragraph, however, the great circles containing Ch and L⊥ tend to be inclined at moderate to high angles to the fabric axis b, rather like in the case of the lamellae in subareas A, C, F and G. Therefore, it is not apparent whether the lamellae in subarea H are correlated with those in subareas A, C, F and G or those in subareas D and E.

On the basis of the above descriptions and considerations, the right limb of fold C (fold C′) can be divided into three domains with reference to deformation style of quartz grains in the stage of the deformation related to the formation of the lamellae as follows (25-a): domains I and I′ where quartz grains were deformed in such a manner as the Böhm lamellae were not formed in any quartz grain but probably the undulatory extinction would have been formed in many grains, as in domains I and I′ in the stage of the deformation related to the deformation bands, and domain II where quartz grains were deformed in such a manner as the Böhm lamellae, for which in the Ch-L⊥ diagram we can find a familiar regularity, were formed in some grains and the undulatory extinction in many grains. The pattern of the Ch-L⊥ diagram (Fig. 18) indicates that the movement picture in the deformation related to the Böhm lamellae was statistically approximately homogeneous within domain II. As read in Fig. 25-a, the arrangement of those domains on either side of the axial plane of fold C′ are approximately symmetrical. This relationship is similar to that for the deformation bands, as is obvious when Figs. 25-a and 18 are compared with Figs. 15-a and 10, respectively. At this time, points C and T in the diagram for the Böhm lamellae may correspond to those for the deformation bands in dynamic sense.

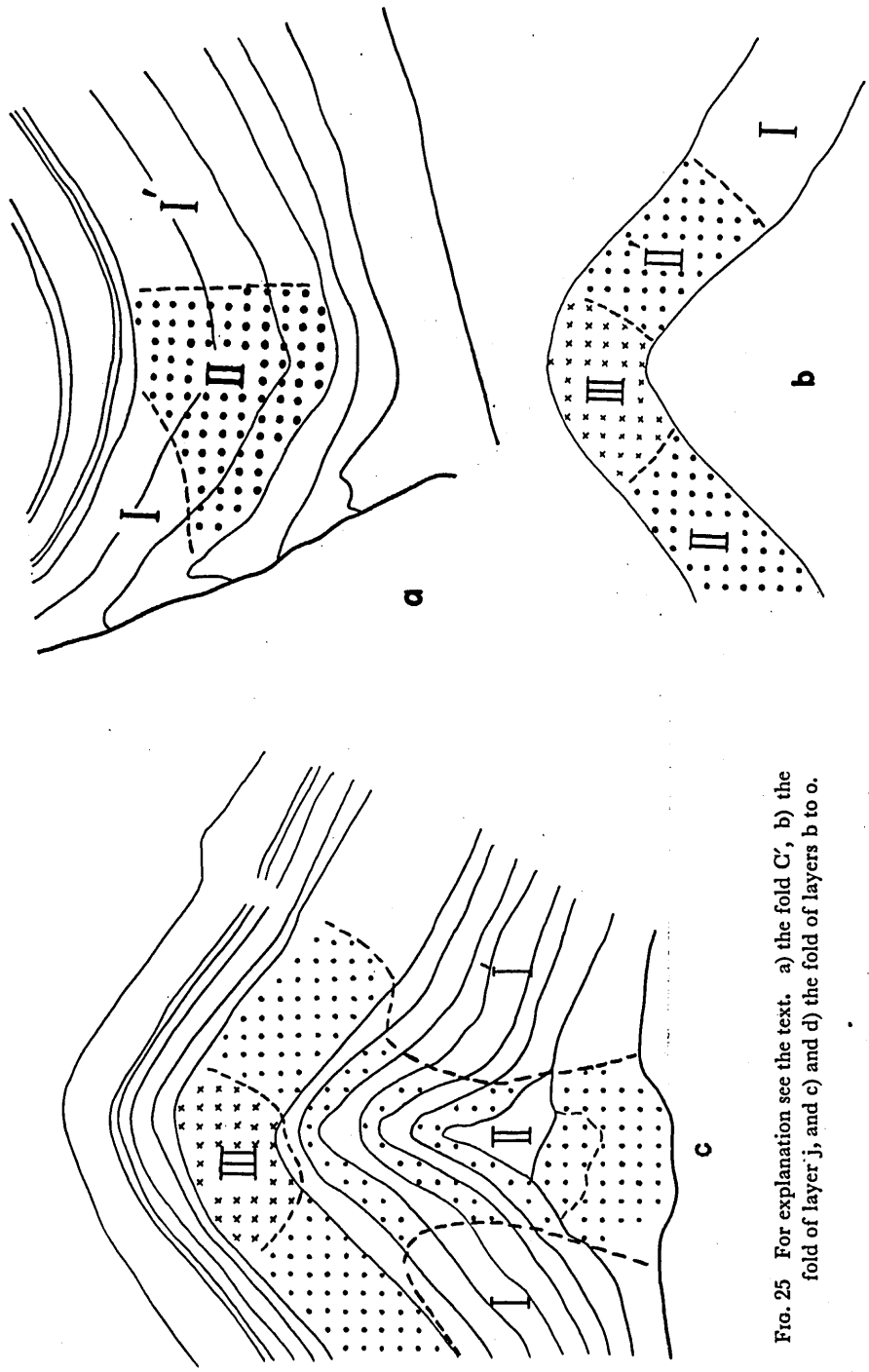


FIG. 25 For explanation see the text. a) the fold C′, b) the fold of layer j, and c) and d) the fold of layers b to o.

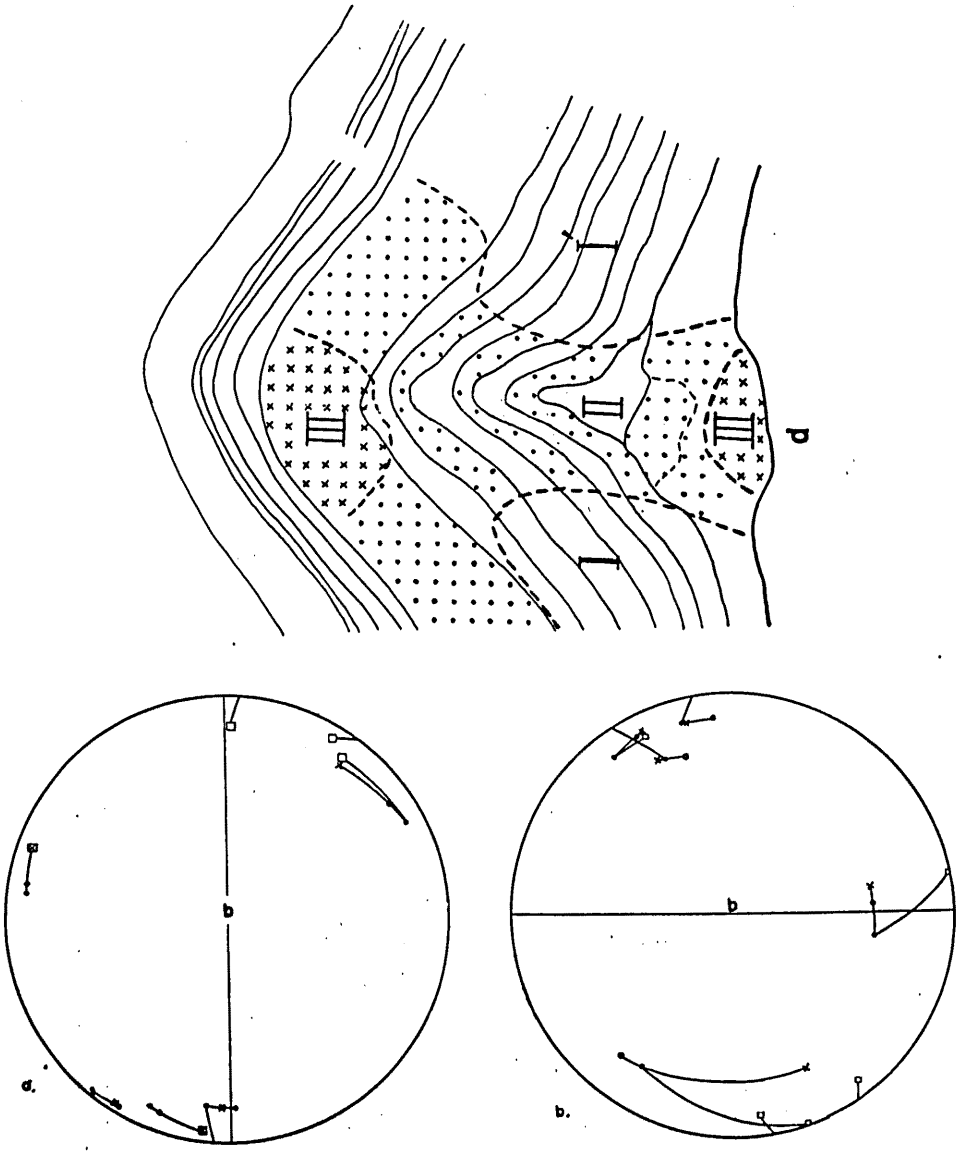


FIG. 26 a) 5 grains containing both Böhm lamellae and deformation bands in subarea A. solid line: the axial plane of fold C'. dots: c-axes of host crystals. circles: c-axes of band crystals for the deformation bands. crosses: poles of the deformation bands (assumed). square: poles of the Böhm lamellae.
b) 5 grains containing both Böhm lamellae and deformation bands in subarea E.

The fold of layer j can be divided into five domains with reference to deformation style of quartz grains in the stage of the deformation related to the Böhm lamellae as follows (Fig. 25-b): domain I where quartz grains were defeormed in such a manner as probably the undulatory extinction was formed in many grains

but not the Böhm lamellae, domains II and II′ (corresponding to subareas F and C) where quartz grains were deformed in such a manner as the lamellae, for which in the Ch-L⊥ diagram we can find a familiar regularity, were formed in some grains and the undulatory extinction in many grains, and domain III (corresponding to subareas D and E) where quartz grains were deformed in such a manner as the lamellae, for which in the Ch-L⊥ diagrams we cannot detect any regularity, were formed in some grains and the undulatory extinction in many grains. The pattern of the Ch-L⊥ diagrams (Figs. 19 and 22) indicates that the movement picture in the deformation related to the lamellae was statistically approximately homogeneous within each of domains II and II′, and these domains are correlated with domain II in fold C′. As read in Fig. 25-b, the arrangement of those domains on either side of the axial plane are approximately symmetrical.

If the Böhm lamellae in subarea H are correlated with the type of the Böhm lamellae in subareas A, C, F and G, we can make a diagram, Fig. 25-c, with reference to deformation style of quartz grains in the stage of the deformation related to the Böhm lamellae. On the other hand, if the lamellae in subarea H are correlated with the type of the Böhm lamellae in subareas D and E, we can make another diagram, Fig. 25-d. Domains I, I′, II and III in Fig. 25-c and d correspond to those in Fig. 25-a and b respectively.

Now, following points come into question: 1) What is the meaning of Fig. 25-a, b, c and d? 2) What is the cause of the fact that quartz grains containing the Böhm lamellae are not found in the quartz-rich layers of the left limb of fold C and in the quartz-rich layers l, n, p and r involved in fold B. The distribution of quartz grains containing the Böhm lamellae through the fold is essentially the same as that of the deformation bands, though the former is slightly more enlarged than the latter, as is obvious when Plate 34-4 is compared with Plate 34-3. Therefore, above-described problems may be roughly explained in the same terms as those for similar problems on the deformation bands mentioned in the preceding pages. At present, however, it seems to be difficult to discuss more deeply those problems. Generally, the Böhm lamellae referred to the type of the lamellae of domains II and II′ and those to that of domain III appear to be confused in the specimens previously described by many authors.

## References

Bailey, S. W., Bell, R. A. and Peng, C. J. (1958): Plastic deformation of quartz in nature. *Geol. Soc America Bull.*, **69**, 1443-1460.

Carter, N. L., Christie, J. M. and Griggs, D. T. (1961): Experimentally produced deformation lamellae and other structures in quartz sand (abstract). *Jour. Geophys. Reseach*, **66**, 2518-2519.

Christie, J. M. and Raleigh, C. B. (1959): The origin of deformation lamellae in quartz. *Am. Jour. Sci.*, **257**, 385-407.

Christie, J. M., Carter, N. L. and Griggs, D. T. (1962): Plastic deformation of single crystals of quartz (abstract). *Jour. Geophys. Reseach*, **67**, 3549-3550.

CONRAD, H. (1961): The role of grains boundaries in creep and stress rupture. (in *Mechanical behaviour of metals at elevated temperatures*, edited by J. Dorn). McGraw-Hill Book Company, Inc.

FAIRBAIRN, H. W. (1941): Deformation lamellae in quartz from the Ajibik formation, Michigan. *Geol. Soc. America Bull.*, **52**, 1265-1277.

HANSEN, E. C. and BORG, I. Y. (1962): The dynamic significance of deformation lamellae in quartz of a calcite-cemented sandstone. *Am. Jour. Sci.*, **260**, 321-336.

HARA, I. (1961a): Dynamic interpretation of the simple type of calcite and quartz fabrics in the naturally deformed calcite-quartz vein. *Jour. Sci. Hiroshima Univ. Series* C, **4**, 35-54.

——— (1961b): Petrofabric analysis of the lamellar structures in quartz. *Jour. Sci Hiroshima Univ. Series* C, **4**, 55-70.

——— (1963): Petrofabric analysis of a drag fold. *Geol. Rep. Hiroshima Univ.*, **12**.

HERITSCH, H. and PAULITSCH, P. (1954): Ueber einen Schriftgranit von Radegund bei Graz. *Tschermaks Mineralog. Petrog. Mitt.*, F. 3, Bd. IV, 18-27.

INGERSON, E. and TUTTLE, O. F. (1945): Relations of lamellae and crystallography of quartz and fabric directions in some deformed rocks. *Am. Geophys. Union Trans.*, **26**, 95-105.

RAMBERG, H. (1952): *The origin of metamorphic and metasomatic rocks.* The University of Chikago Press.

——— (1961): Relationship between concentric longitudinal strain and concentric shearing strain during folding of homogeneous sheets of rocks. *Am. Jour. Sci.*, **259**, 382-390.

RILEY, N. A. (1947): Structural petrology of the Baraboo quartzite. *Jour. Geology*, **55**, 453-475.

SANDER, B. (1930): *Gefügekunde der Gesteine.* Vienna, Springer Verlag.

SITTER, L. U. de (1956): *Structural gelogogy.* New York.

SULLY, A. H. (1956): Recent advances in knowledge concerning the progress of creep in metal. *Progress in metal physics*, **6**, 135-180.

TURNER, F. J. and WEISS, L. E. (1963): *Structural analysis of metamorphic tectonites.* MacGraw-Hill Book Company, Inc.

INSTITUTE OF GEOLOGY AND MINERALLOGY
FACULTY OF SCIENCE, HIROSHIMA UNIVERSITY

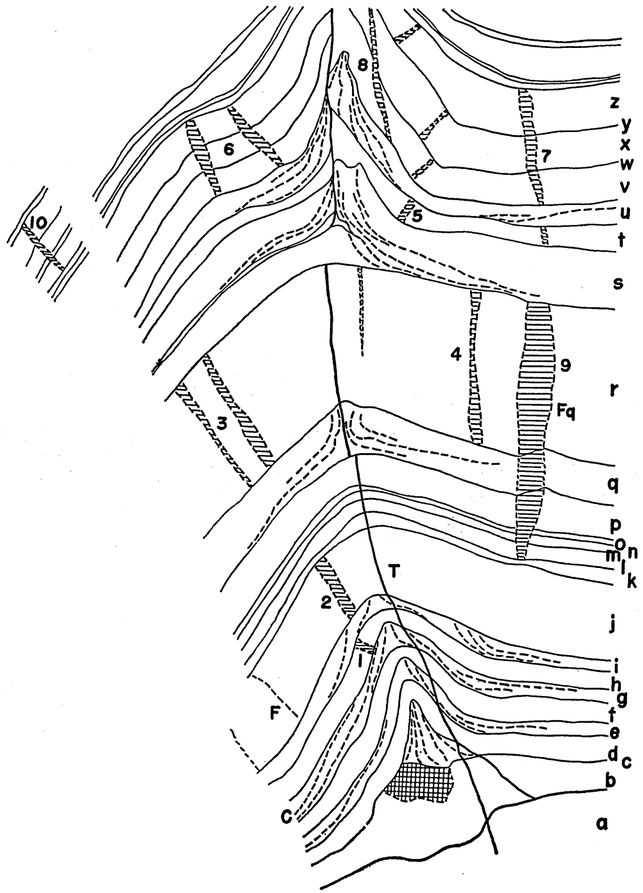


FIG. 1. Sketch of the fold on the plane of thin section normal to the fold-axis. a, b, c, ..... : names of layers. C : transversal slip cleavages in the mica-rich layers. T : fracture plane along the axial plane of the fold. 1, 2, 3, ..., 10 : numbers of the Fq zone. F and Fq : For explanation see the text.

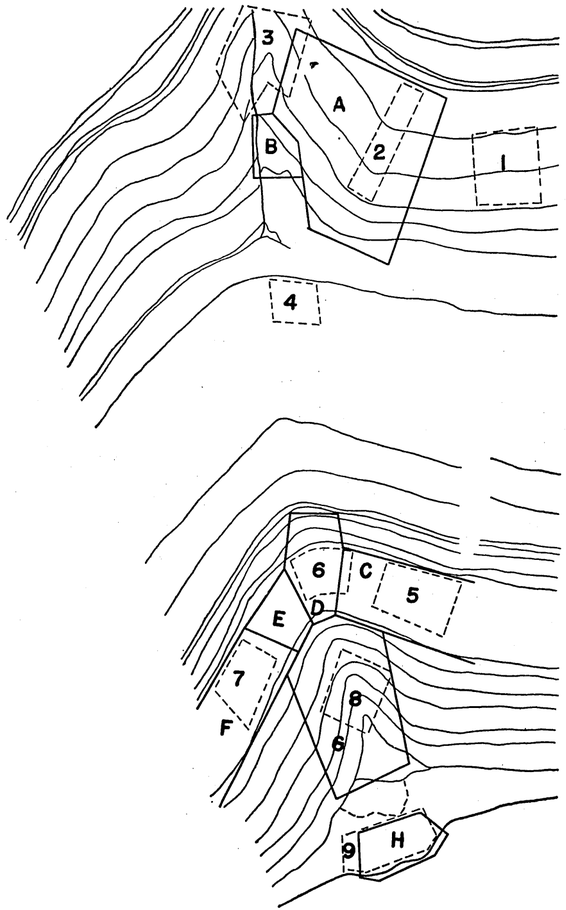


FIG. 2. Diagram of fold showing position of 9 sectors (dotted line) where the quartz c-axis fabric has been examined, and position of 8 subareas (solid line) where the Böhm lamellae and deformation bands have been found.

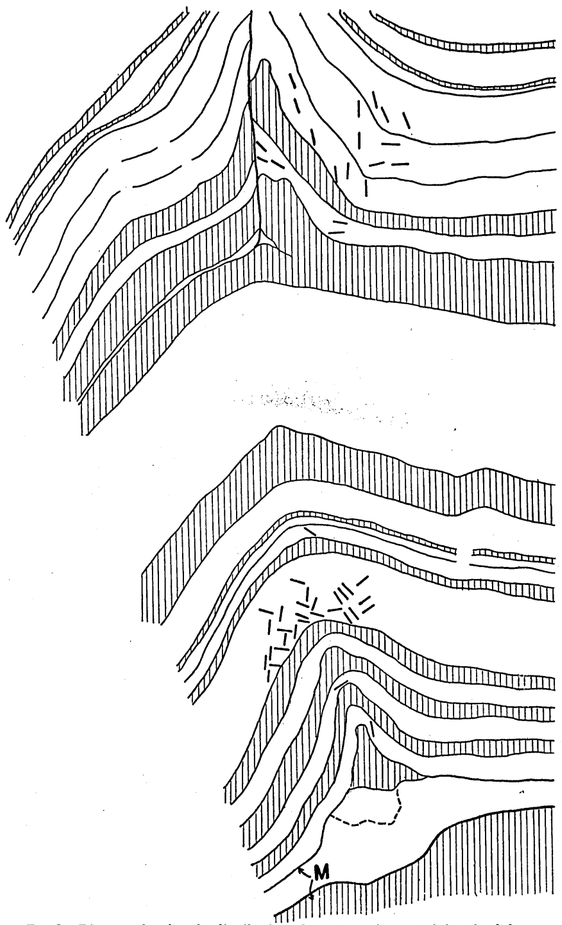


FIG. 3. Diagram showing the distribution of quartz grains containing the deformation bands through the fold and the trend of the bands in each grain, analysed on the thin section normal to the fold-axis. M : the mica-rich layer.

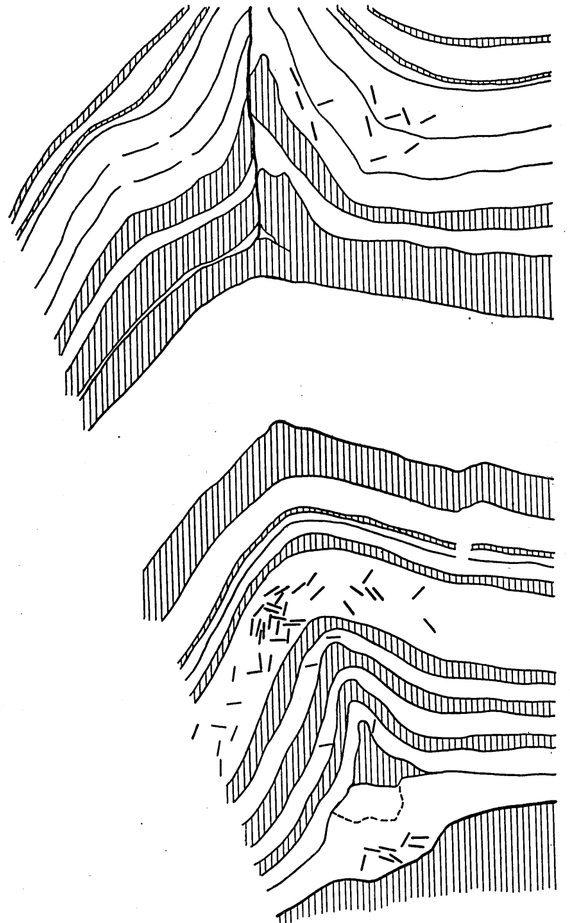

FIG. 4. Diagram showing the distribution of quartz grains containing the Böhm lamellae through the fold and the trend of the lamellae in each grain, analysed on the thin section normal to the fold-axis.

## Explanation of Plate XXXV

Fig. 1 Fq zone 2, photographed on the plane of thin section normal to the fold-axis. Lower nicol only.

All figures in following Plates are photographed on the plane of thin section normal to the fold-axis.

Fig. 2 ditto. Crossed nicols.

Fig. 3 Fq zone 7. Crossed nicols.

Fig. 4 Fq zone 4. Crossed nicols.

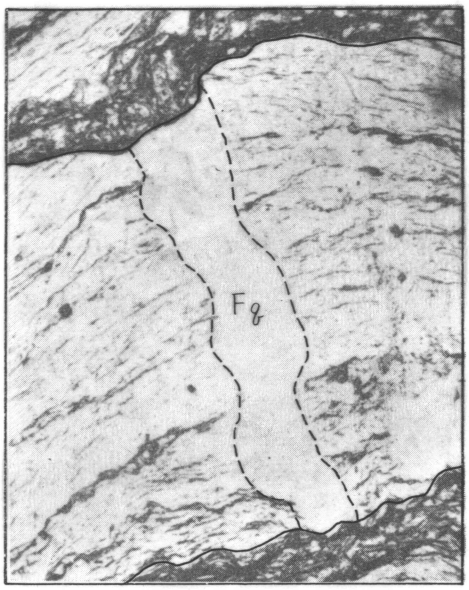


FIG. 1

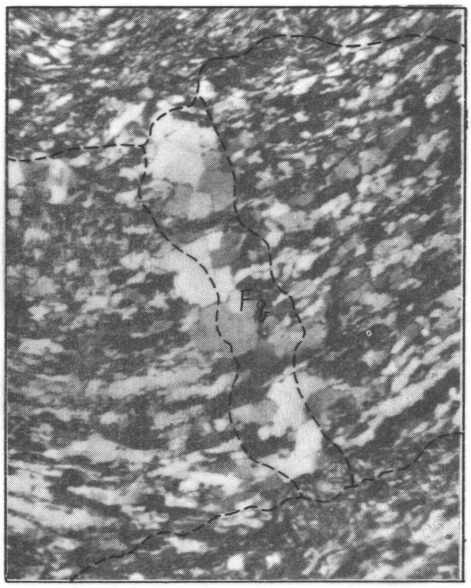


FIG. 2

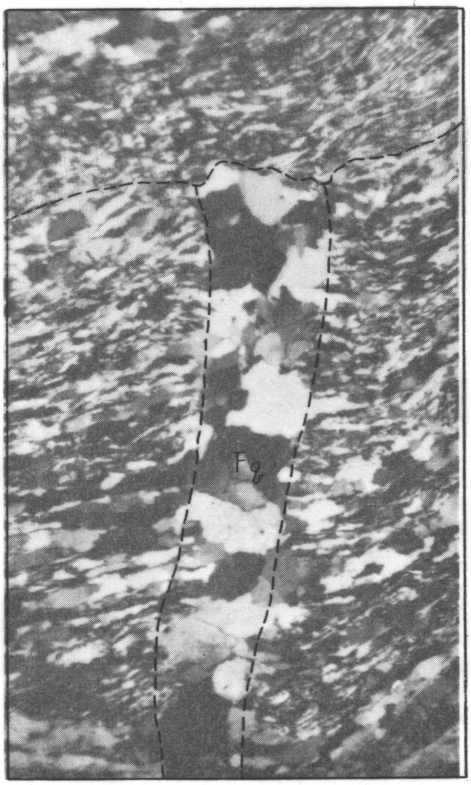


FIG. 3

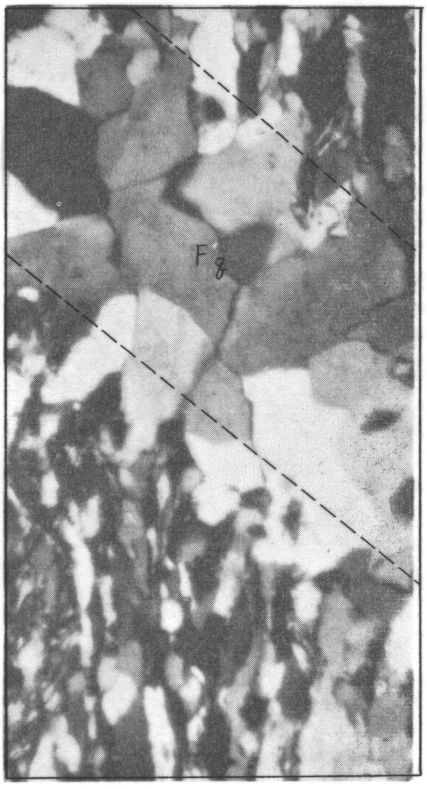


FIG. 4

FIG. 1

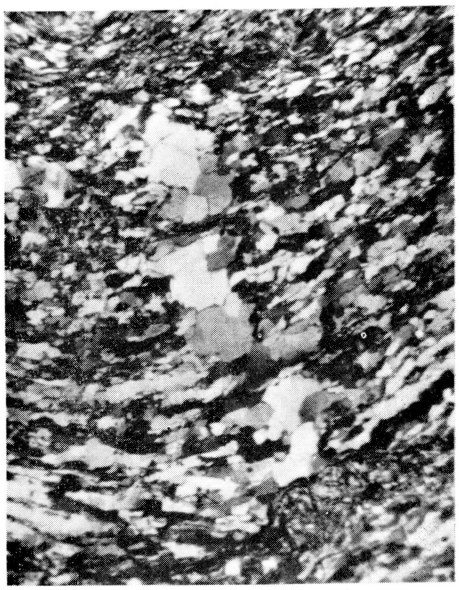

FIG. 2

FIG. 3

FIG. 4

## Explanation of Plate XXXVI

Fig. 1 Fq zone 10. Lower nicol only.
Fig. 2 ditto. Crossed nicols.
Fig. 3 Fq zone and F-surface. Crossed nicols.
Fig. 4 ditto. Lower nicol only.

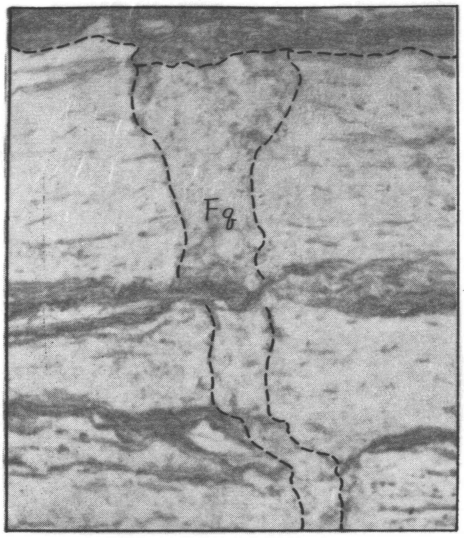


FIG. 1

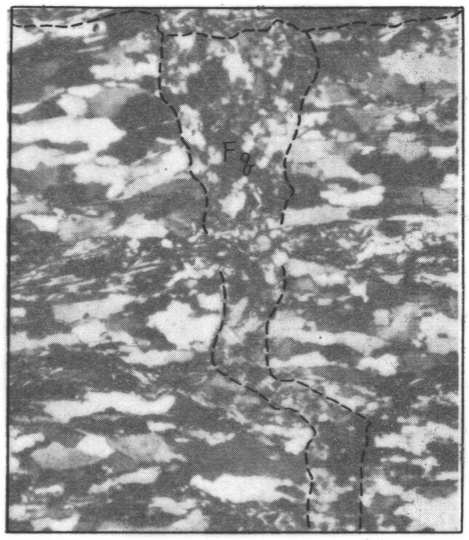


FIG. 2

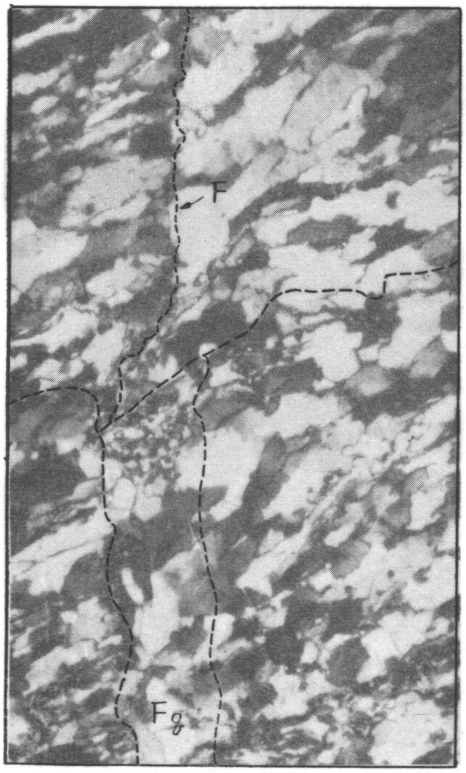


FIG. 3

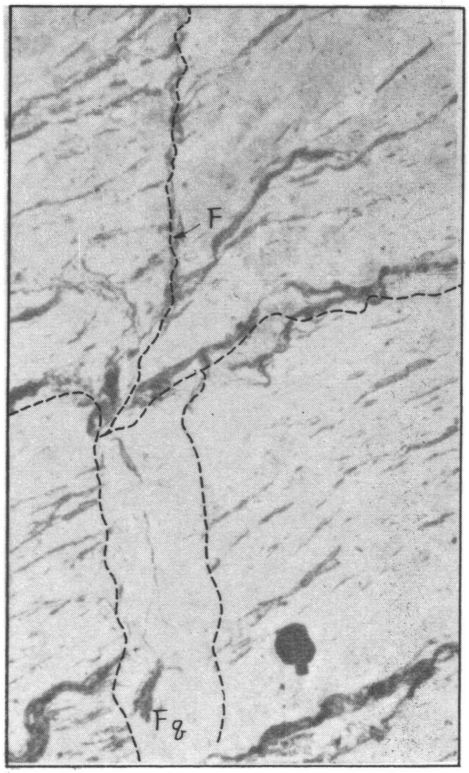


FIG. 4

FIG. 1

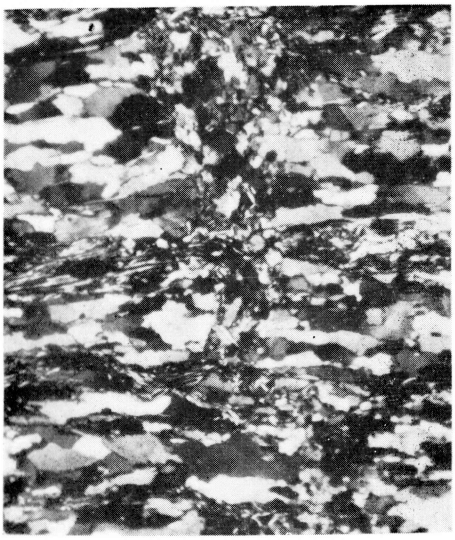

FIG. 2

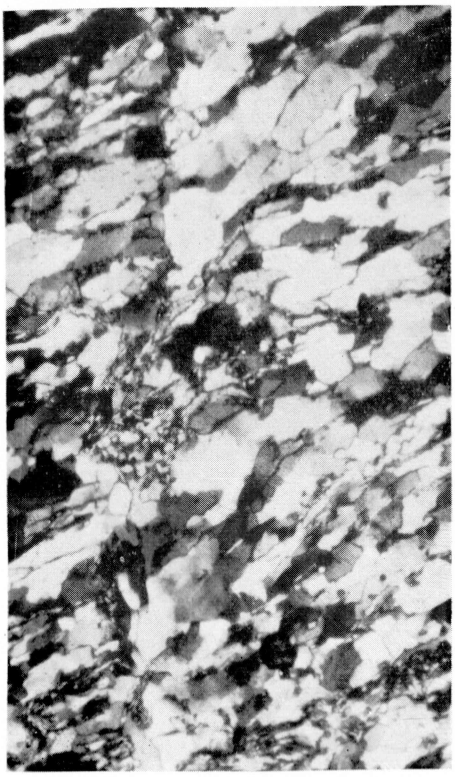

FIG. 3

FIG. 4

## Explanation of Plate XXXVII

Fig. 1 Fq zone 9. o, p and q : name of layer. I and II : two subzones, that is, the former consists of coarse granular grains of quartz and the latter of row of voids free from quartz grains and other mineral grains. Lower nicol only.

Fig. 2 ditto. Crossed nicols.

Fig. 3 Fq zone 8. Lower nicol only.

Fig. 4 Inner knee of fold A. b, c and d : name of layer. Crossed nicols.

Fig. 5 F-surface. Lower nicol only.

Fig. 6 ditto. Crossed nicols.

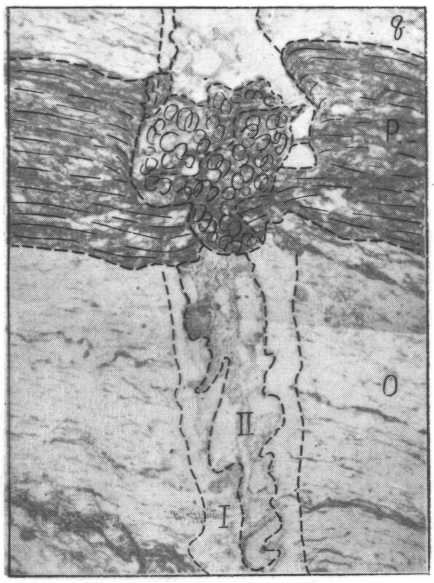


FIG. 1


FIG. 2

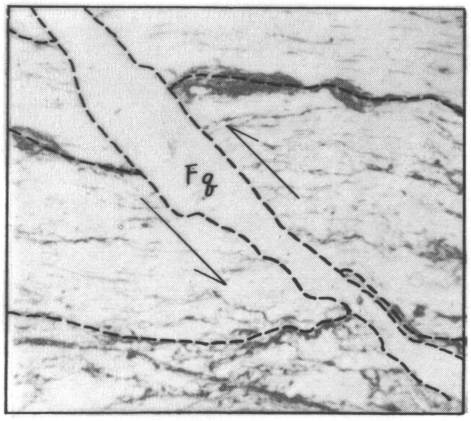


FIG. 3

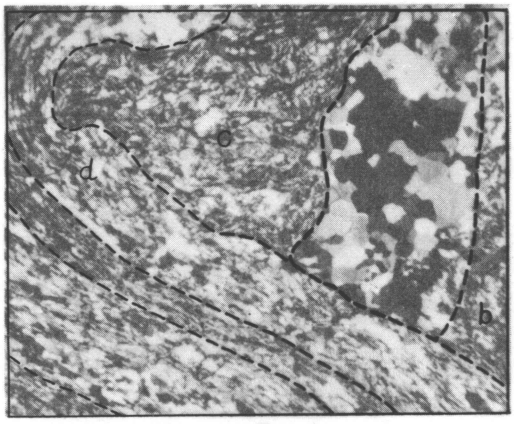


FIG. 4

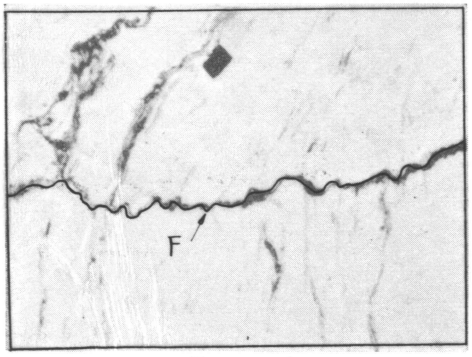


FIG. 5

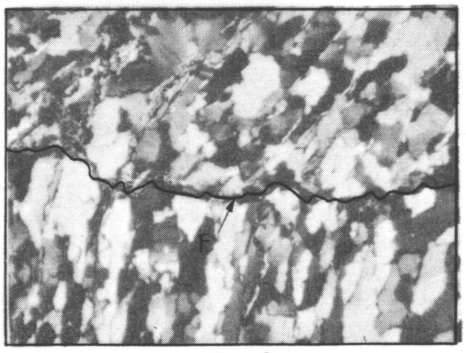


FIG. 6

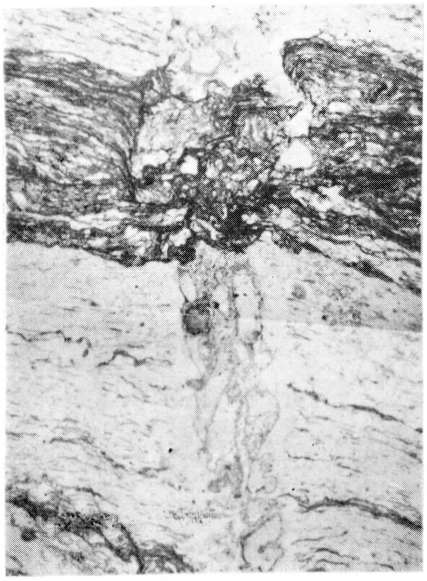

FIG. 1

FIG. 2

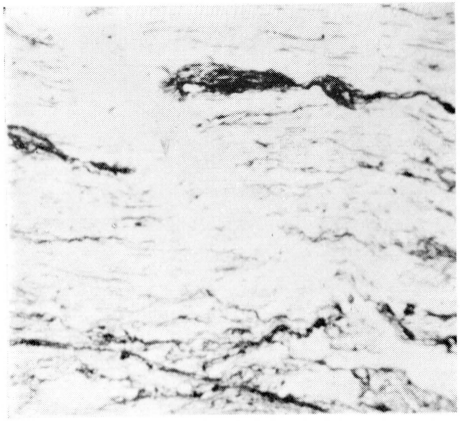

FIG. 3

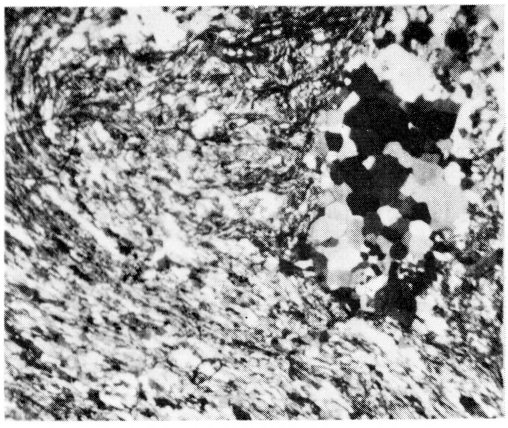

FIG. 4

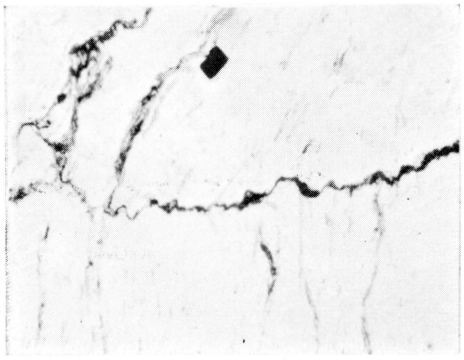

FIG. 5

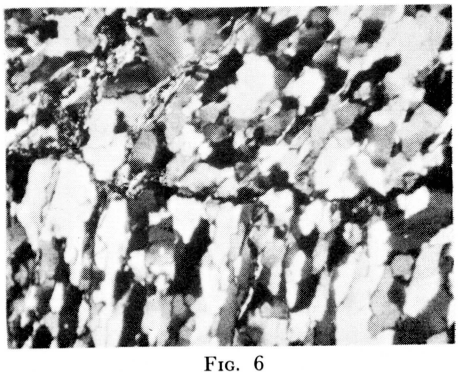

FIG. 6

## Explanation of Plate XXXVIII

Fig. 1 F-surface, a part of that shown in Fig. 3 of Plate 36. Crossed nicols.
Fig. 2 ditto. Lower nicol only.
Fig. 3 F-surface. Lower nicol only.

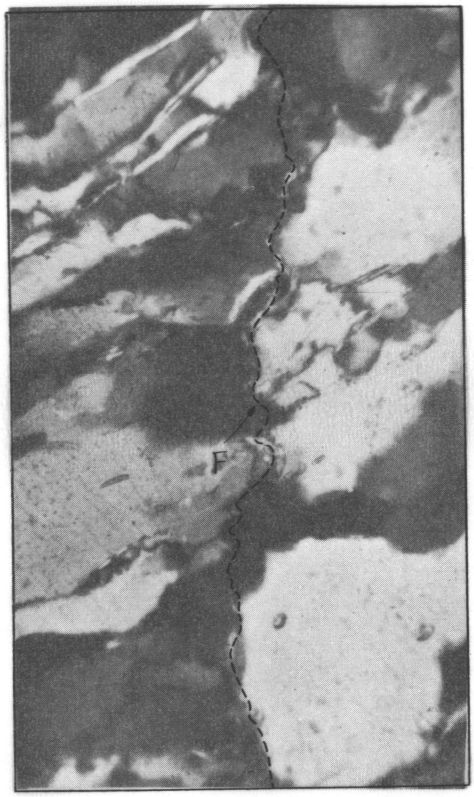


FIG. 1


FIG. 2

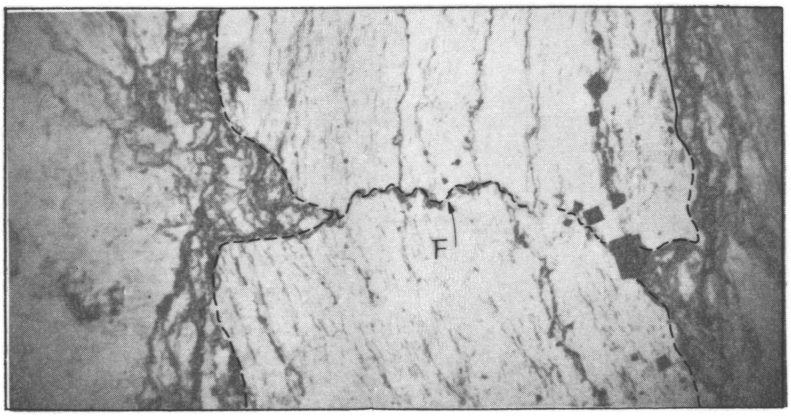


FIG. 3

FIG. 1

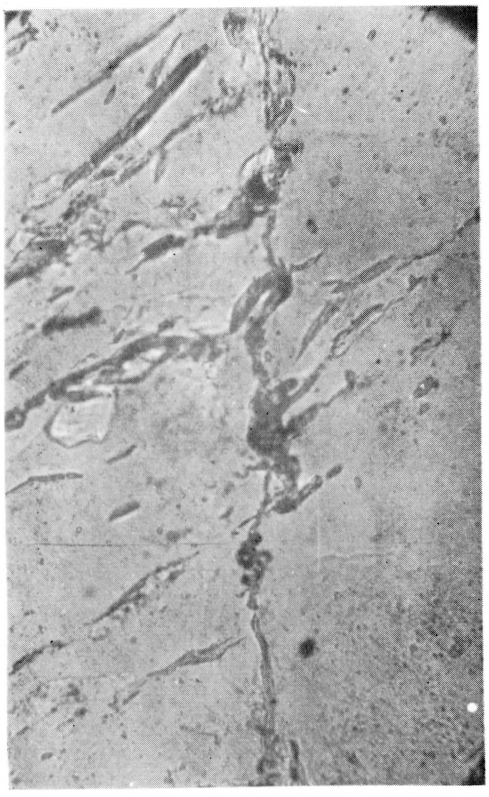

FIG. 2

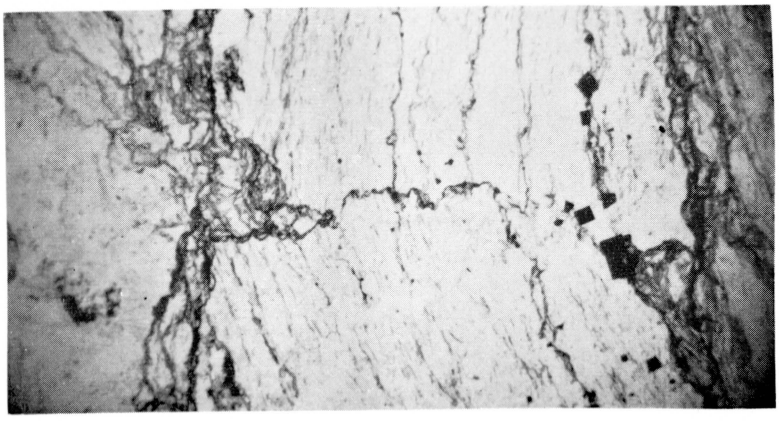

FIG. 3

## Explanation of Plate XXXIX

Fig. 1 F-surface, a part of that shown in Plate 37-5 and 6. Lower nicol only.
Fig. 2 ditto. Crossed nicols.
Fig. 3 F-surface, a part of that shown in Plate 38-3. Lower nicol only.
Fig. 4 ditto. Crossed nicols.

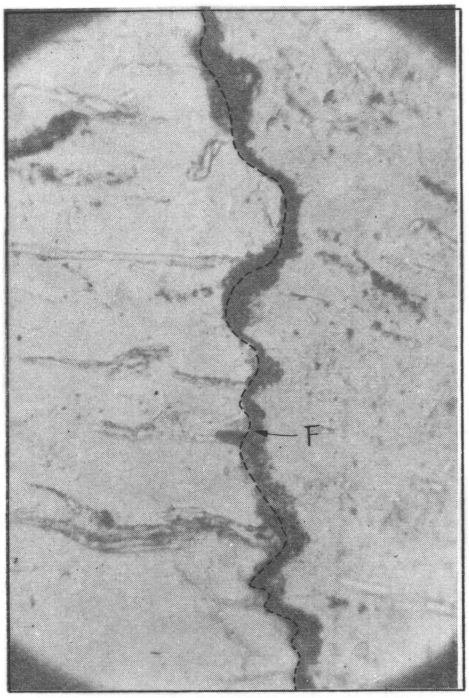


FIG. 1

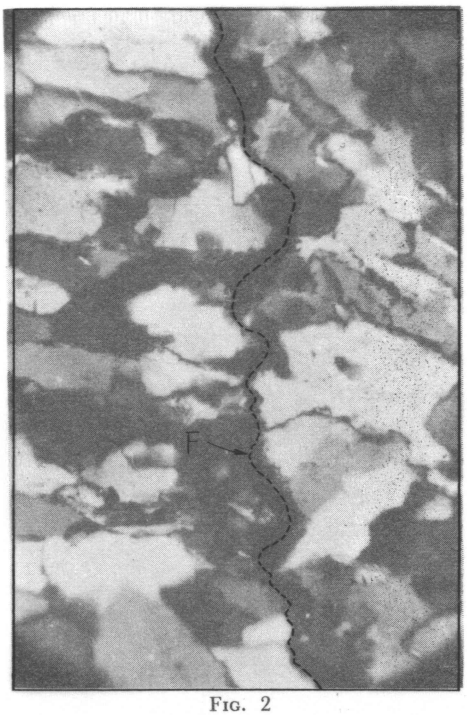


FIG. 2

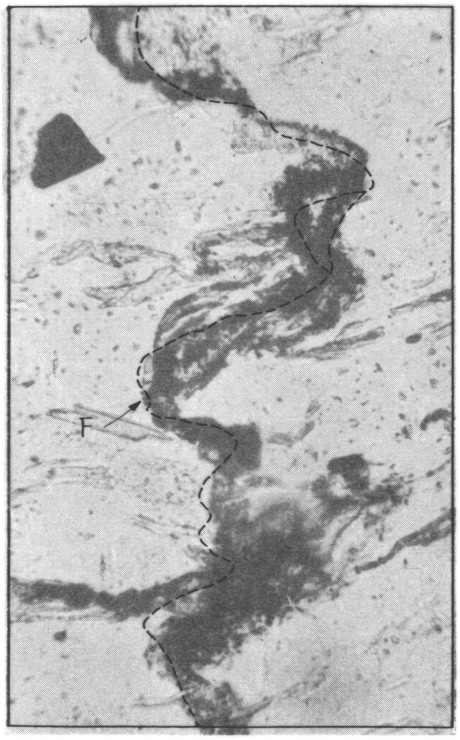


FIG. 3

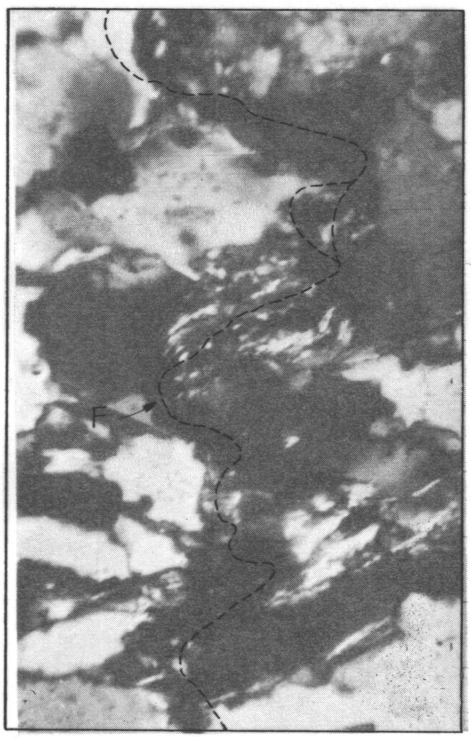


FIG. 4

FIG. 1

FIG. 2

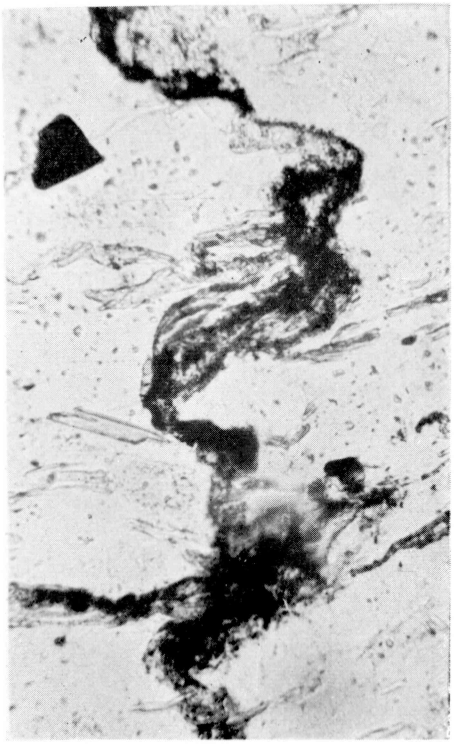

FIG. 3

FIG. 4

## Explanation of Plate XL

Fig. 1 Böhm lamellae. Crossed nicols.
Fig. 2 Böhm lamellae and deformation bands in the same grain. Crossed nicols.
Fig. 3 Deformation bands in one grain and Böhm lamellae in other grain. Crossed nicols.
Fig. 4 Fracture plane along the axial plane of the fold. Crossed nicols.

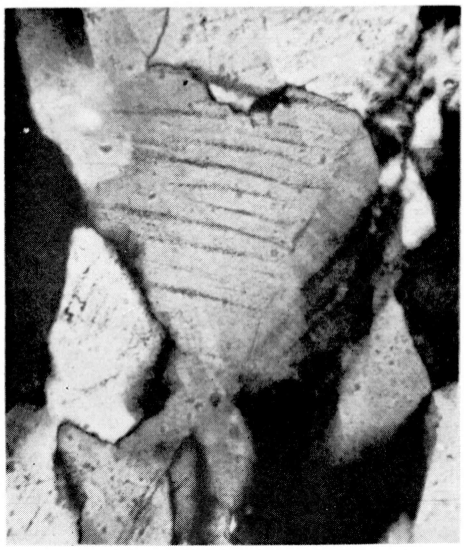

FIG. 1

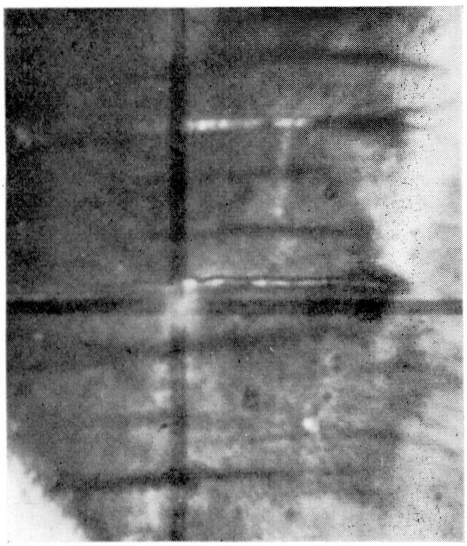

FIG. 2

FIG. 3

FIG. 4